GaAs spin polarized electron source

D. T. Pierce, R. J. Celotta, G.-C. Wang, W. N. Unertl,[a] A. Galejs, C. E. Kuyatt, and S. R. Mielczarek

National Bureau of Standards, Washington, D.C. 20234

(Received 3 December 1979; accepted for publication 4 January 1980)

The design, construction, operation, and performance of a spin polarized electron source utilizing photoemission from negative electron affinity (NEA) GaAs are presented in detail. A polarization of $43\pm2\%$ is produced using NEA GaAs (100). The polarization can be easily modulated without affecting other characteristics of the electron beam. The electron beam intensity depends on the intensity of the exciting radiation at 1.6 eV; beam currents of 20 μA/mW are obtained. The source is electron optically bright; the emittance phase space (energy-area-solid angle product) is 0.043 eV mm^2 sr. The light optics, electron optics, and cathode preparation including the GaAs cleaning and activation to NEA are discussed in depth. The origin of the spin polarization in the photoexcitation process is reviewed and new equations describing the depolarization of photoelectrons in the emission process are derived. Quantum yield and polarization measurements for both NEA and positive electron affinity surfaces are reported. The important considerations for interfacing the polarized electron source to an experiment are illustrated by its application to polarized low energy electron diffraction (PLEED). The advantages of this spin polarization modulated electron gun for PLEED are clearly demonstrated by sample PLEED results for W(100) and ferromagnetic Ni(110). A comparison with other polarized electron sources shows that the GaAs spin polarized electron source offers many advantages for a wide range of applications.

PACS numbers: 29.25.Bx

INTRODUCTION

A. Background

Better sources of spin polarized electrons have been desired for many years. Some pioneering experiments have been carried out at great difficulty with marginal sources, but there remains a backlog of proposed measurements awaiting improved spin polarized electron sources. In the last decade, as new types of sources have emerged, there has been a large increase in proposals for applications of spin polarized electrons.

Improved sources developed recently exploit a variety of physical processes including chemi-ionization of optically oriented He(2^3S) atoms in a He afterglow,[1] the Fano effect in Rb[2] and Cs,[3] photoionization of polarized Li atoms,[4] field emission from W-EuS tips,[5] photoemission from the ferromagnetic crystal EuO,[6] and, the topic of this paper, photoemission from GaAs. There are many applications of polarized electron sources in solid state physics. Polarized low energy electron diffraction (PLEED) is being explored for surface structure determination. Studies of exchange scattering from ferromagnetic surfaces will provide a measure of surface magnetization and its dependence on temperature and adsorbates. Both spin-orbit and spin-exchange effects have been considered as sources of the spin dependence of electron scattering in atomic physics where the theoretical activity has been far greater than for solids. Improved sources will allow "complete scattering" experiments to be carried out where scattering amplitudes and relative phases are measured. Such experiments severely test theoretical models including, in the case of the spin-orbit interaction, the relativistic parts. This is desirable for extrapolation of the theoretical models to important practical situations. In nuclear physics and high energy physics polarized electrons are of interest for studying parity violating neutral current interactions.[7] Measurements of the polarization asymmetry in the scattering of polarized electrons arising from the interference between weak and electromagnetic interactions provide tests of proposed unified gauge theories.

In 1974, at the ETH-Zurich, a new type of spin polarized source based on photoemission from GaAs was proposed.[8] Subsequently, a Mott detector was used to measure the spin polarization of electrons photoemitted from GaAs, which had the electron affinity lowered by the application of cesium and oxygen. A polarization of about 40% was measured. The sign of the polarization could be rapidly and easily reversed by changing the handedness of the circularly polarized light used to photoexcite the electrons. The lowered electron affinity allows an intense electron beam to be obtained. The results of these experiments have been described in detail elsewhere.[9–11]

The experiments in Zurich were carried out on a large apparatus designed specifically for spin polarized photoemission measurements.[12] The purpose of this paper is to describe how this effect can be used to provide a compact spin polarized electron gun which provides an intense beam of constant intensity with a spin polarization that can be sinusoidally (or other-

 0034-6748/80/040478-22$00.60

wise) modulated at a desired frequency. The polarized electron source we will describe has now become a practical device and is being applied routinely to study polarized electron scattering from surfaces.

At NBS we have focused on developing a continuous current source for low energy (0–1000 eV) applications. In parallel with our source development, a group at the Stanford Linear Accelerator Center developed[13] a pulsed source for injection at 70 keV into the two-mile linear accelerator. Both groups frequently encountered similar problems in the course of the source development; we are grateful for the cooperation with the SLAC group which speeded the development of the sources.

The attractiveness of the GaAs source is evident in its early applications. The NBS source has been applied to scattering of low energy electrons from crystal surfaces, i.e., polarized low energy electron diffraction (PLEED). Since the beam incident on the surface has constant intensity but changing polarization, any intensity change in the scattered beam in phase with the polarization modulation is a direct measure of the spin dependence of the scattering. Spin-dependent scattering has been observed due to the spin–orbit interaction in the case of W(100)[14] and due to the exchange interaction in the case of ferromagnetic Ni(110).[15] The SLAC source has been applied to measure parity nonconservation in inelastic scattering from hydrogen and deuterium.[16] The high intensity of the GaAs source and the possibility of rapid polarization reversal without changing the electron beam characteristics were crucial to the experiment.

B. Requirements of a polarized electron source

A number of parameters characterize a source of spin polarized electrons, and each application has its own requirements. The quantity P^2I, where P is the polarization and I is the beam current, is often used as a figure of merit in discussing polarized electron sources. This figure of merit applies when counting statistics are the chief source of experimental uncertainty. However, because of systematic errors, some minimum P is required to make the measurements. It is not always possible to trade off P and increase I. The beam current at some point will be limited by space charge or the beam current may be intentionally limited to avoid beam induced target damage. Thus, there are many situations where a high P is necessary.

The time structure of both the polarization and intensity is important. Most experiments require that the polarization of the incident beam be reversible. The possibility of modulating the polarization at a desired frequency or with arbitrary time structure can be a significant advantage. Another important consideration is the effect of polarization reversal on the position, angle, intensity or energy of the beam. Sources in which a magnetic field must be reversed in order to reverse the polarization are less desirable because the field cannot be switched rapidly or without disturbing the beam.

Another consideration is whether the polarization is longitudinal or transverse, that is, whether it lies along or perpendicular to the electron momentum. However, a rotation from longitudinal to transverse polarization and vice versa is readily achieved with a 90° electrostatic deflection or by using a Wien filter (crossed electric and magnetic fields).

The electron optical characteristics of the polarized electron beam determine how much of the beam can be accepted by other devices such as an energy analyzer or a detector. In the paraxial beam approximation, the energy-area-solid angle phase space product, $EA\Omega$, of the beam is conserved. That is, $E_1A_1\Omega_1 = E_2A_2\Omega_2$ for any two cross sections 1 and 2 along the beam. At a given point along the beam, E is the electron kinetic energy, A is the cross-sectional area, and Ω is the solid angle subtended by the electron beam envelope. When a magnetic field is present, such as when the beam originates at a magnetic photocathode, the situation is more complicated and has been discussed in detail elsewhere.[17] If the acceptance phase space product of an electron optical device $(EA\Omega)_d$ is smaller than that of the incident beam $(EA\Omega)_i$, the beam current is reduced by the ratio $(EA\Omega)_d/(EA\Omega)_i$. A high current beam with a large $EA\Omega$ may not be as useful as a lower current beam with much smaller $EA\Omega$. Thus, $EA\Omega$ is an electron optical figure of merit for the polarized electron source. One often hears reference to electron optical brightness which is defined as $\mathcal{B} = dI/dAd\Omega$, where dI is the differential current through a differential area dA and $d\Omega$ is the differential solid angle subtended by the beam at dA. Since $EA\Omega$ is conserved, $\mathcal{B}/E$ is also a conserved quantity.

The emittance is defined as $\epsilon = RR'$, where R is the radius of the electron beam at the source or an image of the source and R' is the cone half-angle of the electron beam envelope at that point. The emittance invariant, ϵ_{inv}, is defined as $RR'\sqrt{E}$, and serves the same purpose as $EA\Omega$, since $EA\Omega = \pi^2\epsilon_{\text{inv}}$. The energy distribution of the electrons is also an important parameter and must be considered when specifying the source.

Finally, the stability of the polarization and current from the source is important. One can distinguish between short-term stability, such as fluctuations during a measurement, and long-term stability or drifts.

C. Overview of the operation of the GaAs source

An overview of the source operation can be obtained by referring to Fig. 1, which shows a schematic of the polarized electron gun attached to a surface analysis chamber. There are several key elements for the operation of the polarized electron source, which we discuss in detail in the subsequent sections.

The spin polarized photoelectrons are excited by circularly polarized light of photon energy just greater

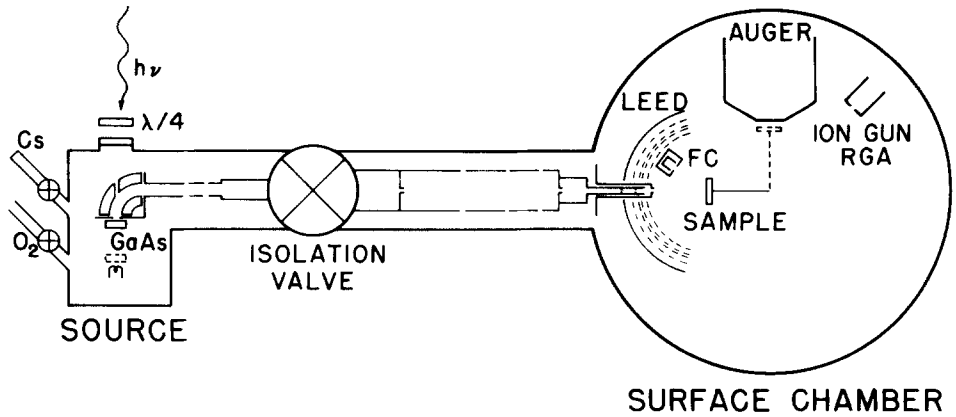

FIG. 1. Overview of the GaAs source, showing it connected through an isolation valve to an experimental chamber for PLEED. Modulating the handedness of the circular polarized light incident on the GaAs produces a constant-intensity photoelectron beam with a modulated spin polarization. The ac component of the intensity of the electron beam scattered from the sample to the Faraday cup, synchronous with the spin polarization modulation, measures the spin-dependent scattering.

than the bandgap of the GaAs photocathode. The electron spin polarization is reversed by changing the handedness of the circularly polarized light by rotating a quarter wave plate. The two light sources we have used (a Zr arc and a GaAlAs diode laser), the optics to focus the light on the crystal, ways to obtain circularly polarized light, the measurement of the circular polarization, and our set up for quantum yield measurements will be described in Sec. I.

Electrons excited to the conduction band minimum are normally prevented from escaping from the crystal by its high electron affinity, ~4 eV in GaAs. However, GaAs has the very favorable property that the vacuum level can be lowered below the bulk conduction band minimum by application of Cs and O_2. This condition is called negative electron affinity (NEA). NEA surfaces are very efficient photoemitters because the depth from which electrons can be emitted is not limited by the hot electron mean free path (~10 Å) but rather by the diffusion length (~1 μm) for electrons thermalized to the conduction band minimum. In Sec. II we discuss the source chamber and vacuum requirements, the GaAs material requirements, the cleaning of the GaAs, and our activation procedure. Examples of quantum yield curves will be presented.

The theoretical spin polarization of photoelectrons from NEA GaAs is 50% due to the selection rules for excitation with circularly polarized light from the highest of the spin orbit split valence bands. There is the possibility of depolarization in a characteristic spin relaxation time τ_s before the electrons are emitted. Thus, measured polarizations are less than 50% and have recently been observed to be face dependent.[18] It is also possible to prepare surfaces with a slight positive electron affinity (PEA), and such surfaces will be discussed along with the NEA cathodes in terms of polarization and emission intensity. The energy and angular distribution of the electrons are determined by the details of the photoemission process and will be discussed in Sec. III.

The GaAs photocathode comprises the first element of an electron gun which forms a beam and transports it to the interaction region, which in our case is the surface scattering chamber. The initial electron polarization is longitudinal. A 90° spherical electrostatic deflector changes the direction of the electron beam but not the spin direction, thereby giving the transverse polarization required for our scattering experiment. The electron optics and the electron-optical properties of the beam, such as the phase space product $EA\Omega$, will be discussed in Sec. IV.

The overall performance of the source, the parameters describing it, and examples of its application to polarized electron scattering from surfaces will be discussed in Sec. V. A comparison is made between the GaAs source and other available sources.

I. OPTICS

A. Continuum light source

In the development of the polarized electron source, we primarily used a Zr arc lamp[19] which provides an intense continuum with characteristic lines superimposed. The light originates from a spot about 3 mm in diameter. This lamp was used with a monochromator to make quantum yield measurements or with a filter to produce a polarized electron beam. A red filter[20] passed only photon energies below ~1.7 eV (5% and 50% transmission at 700 nm and 715 nm, respectively) to avoid exciting electrons from the spin–orbit split-off valence band (Sec. III).

The optics used to focus the light from the Zr arc onto the GaAs crystal are shown in Fig. 2(a). An arrangement known as Köhler illumination[21] gives a uniformly illuminated image of the aperture on the GaAs. Köhler illumination is readily accomplished in the following way[22]: (i) remove lens (2), in Fig. 2(a), and focus the aperture (3) at the plane of the GaAs (9) by moving lens (7). (ii) Replace lens (2), remove aperture (3), and focus the arc at the focal plane (on the arc side) of lens (7) by moving lens (2). (iii) Replace the aperture. This procedure assures uniform illumination of the second lens and the spot on the GaAs. The magnification is given by the ratio of the distance of lens (7) to the GaAs and the distance of the aperture to lens (7). We typically used a 3-mm diameter aperture demagnified to a 1-mm diameter spot on the GaAs. Approximately 0.5 mW of radiation in the useful spectral range from the GaAs band gap to the filter cutoff reaches the GaAs crystal. The optics are matched to the acceptance (~f/10) determined by the

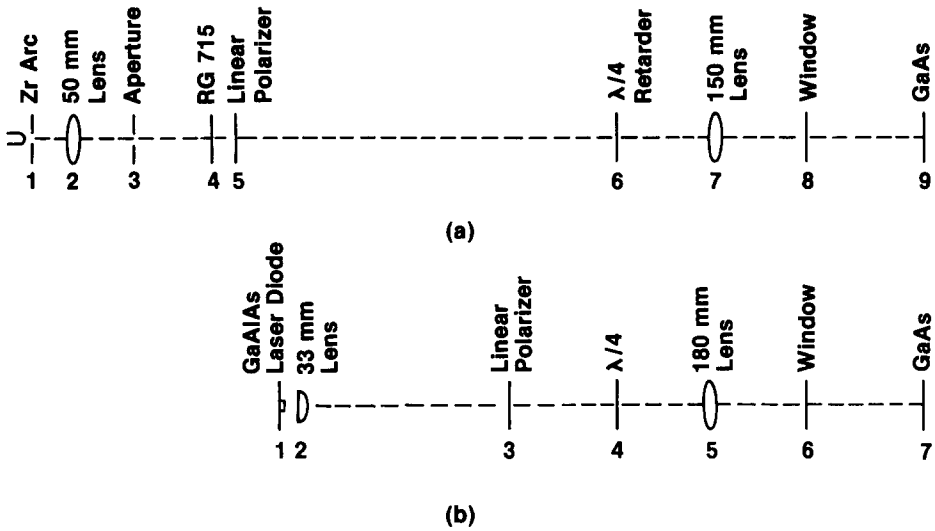

FIG. 2. The arrangement of the optics to provide a focused beam of circularly polarized light on the GaAs photocathode using as a light source a Zr arc (a) and a GaAlAs laser diode (b).

hole through the outer Cu electrode of the 90° electrostatic deflector.

B. GaAlAs laser

For routine use of the polarized electron gun in scattering experiments, we use a GaAlAs injection laser in the CW mode as the light source. Compared to the Zr arc, a smaller more intense light spot of greater stability can be obtained on the GaAs photocathode surface. The band gap of GaAlAs is greater than that for GaAs so that the laser is properly suited to photoexcite electrons to just above the photothreshold of GaAs. Laser diodes with suitable operating wavelengths from 770–820 nm at room temperature can be obtained.[23] With a drive current of 100–200 mA, the laser produces about 10-mW radiation in a bandwidth of 4 nm FWHM. There is a similar increase in the band gap of the GaAs photocathode and the GaAlAs laser on cooling to liquid nitrogen temperature, but we have had mixed success operating the diodes at low temperature. Room temperature operation of the diodes is preferable.

The optical arrangement[24] used with the diode laser is shown in Fig. 2(b). The lens (2) is a 33-mm focal length aspheric lens and is mounted with the laser on the nitrogen reservoir. This prevents temperature shifts of the lens with respect to the laser. A nearly parallel beam is formed which is focused by lens (5), an achromatic doublet, onto the GaAs surface (7). The laser source size is magnified on the GaAs by the ratio of the focal lengths of lens (5) to lens (2). The measured 0.5-mm diameter size of the image on the GaAs is larger than one calculates, probably due to imperfections in the optics.

The laser light intensity is reduced by a factor of 4 in passing through the elements shown in Fig. 2(b). Because too high a light intensity gives space charge limited beams in our LEED gun at low beam energy and also decreases the lifetime of the photocathode, we usually operate with a neutral density filter positioned before the linear polarizer (3) to give 0.5 mW on the photocathode. The light intensity can also be easily decreased by decreasing the diode forward current. The laser radiation is partially linearly polarized.

C. Circular polarization

Circularly polarized light is generated by using a linear polarizer and a quarter wave retarding element. We use a linear dichroic polarizer[25] which has a transmission at 790 nm of about 40%. The light has a linear polarization greater than 99% after passing through the polarizer. The absence of restrictions on angular aperture make such a polarizer well suited to our light sources. We have not detected any deterioration of the polarizer at light flux densities of the order of 1 mW/cm^2, although degradation has been reported[3] for higher flux densities.

For the retarding element we use a mica quarter wave plate. In contrast to higher-order quarter wave retarders made of quartz, for example, the zero-order mica retarder provides approximately quarter wave retardation over a wavelength range of tens of nanometers. As the quarter wave plate rotates, the light goes from right circularly polarized to linear to left circularly polarized, to linear, etc. If the quarter wave plate rotates at frequency ω, the polarization is modulated sinusodially at 2ω. In our apparatus ω is 15 Hz.

If the faces of the quarter wave plate are not parallel, it acts as a rotating wedge and shifts the light beam on the GaAs photocathode surface. This produces an unwanted intensity modulation of the electron beam at ω. Note, however, that motion of the electron beam at ω can also produce an intensity modulation at 2ω if the electron beam crosses back and forth over an aperture. We found it necessary to use specially selected quarter wave plates with faces parallel to within 10 arcsec. It is then possible to modulate the polarization and maintain the position of the light incident on the GaAs such that there is insignificant intensity modulation.

Our use of a motor driven rotating quarter plate is perhaps the simplest approach to modulating the polarization. There are other more sophisticated approaches. The photoelastic modulator[26] has the advantage of a

large angular aperture (50° full cone-angle), but the disadvantage that as an oscillating stress-induced birefringent device it cannot provide static quarter wave retardation. The modulation is sinusoidal and generally at a frequency of tens of kHz. A Pockels cell provides a retardation proportional to the applied voltage. This electro-optic effect has a very fast response time, which allows the polarization to be modulated with arbitrary time structure, an effect used to advantage in the SLAC parity violation experiment.[16] The Pockels cell has a small angular aperture and is therefore suited for use with collimated sources.

The degree of circular polarization of the light is readily measured with a second linear polarizer and a photodiode. With the first linear polarizer and the quarter wave plate fixed, the second linear polarizer is rotated and the maximum intensity I_{MAX} and the minimum intensity I_{MIN} on the photodiode are noted. The degree of circular polarization P_{CP} is[27]

$$P_{CP} = 2(I_{MAX}I_{MIN})^{1/2}/(I_{MAX} + I_{MIN}),$$

where the approximation has been made that the linear polarizers are perfect. A circular polarization of 99% or greater is easily achieved. The handedness can be determined from the position of the fast axis of the retarder relative to the linear polarizer axis. Traditionally in optics, right circular polarization means the electric vector rotates clockwise as seen by an observer facing the light. In particle physics, the helicity is defined by the particle angular momentum with respect to the particle momentum; positive helicity photons correspond to left circularly polarized light in the traditional optics definition. This is useful to note when determining the sign of the spin polarization of the photoelectron beam.

D. Yield measurement

For quantum yield measurements the Zr arc was used as shown in Fig. 2(a). Elements 3–6 are replaced by the monochromator, the entrance slit of which forms the aperture. A calibrated photodiode is placed in the light beam beyond the monochromator to measure the incident light intensity and removed to allow measurement of the photocurrent from the GaAs. Care was taken to be sure all of the light was focused on the GaAs surface; no correction was made for the approximately 15% loss due to the lens and vacuum chamber window. We used a 0.25-m Ebert grating monochromator with 1-mm slits giving a 5-nm resolution. Appropriate filters were used to prevent higher-order diffracted wavelengths from introducing spurious effects near photothreshold where the yield is low. The electrodes in front of the GaAs were biased at +100 V, which was found to be sufficient to collect all of the photoelectrons. The quantum yield measurement, as we shall see below, is very useful in characterizing the photocathode surface.

E. Millilumen source

For activating GaAs with Cs and O_2, we found it helpful to compare our results with those reported from other laboratories. Traditionally photocathodes have been described in terms of their luminous sensitivity, i.e., their response in the wavelength range where the human eye is sensitive. Although this would appear to be an illogical way to describe a photocathode when the interest is in the sensitivity in the near infrared, it is nevertheless current practice. We constructed a special light source consisting of a W filament lamp (filament temperature of 2850 K) which was collimated so that the luminous flux was about 1 mlm.[28] This was determined initially by an intercomparison[29] and subsequently by a photodiode with a photometric filter. The photocathode sensitivity in μA/lm is thereby easily measured.

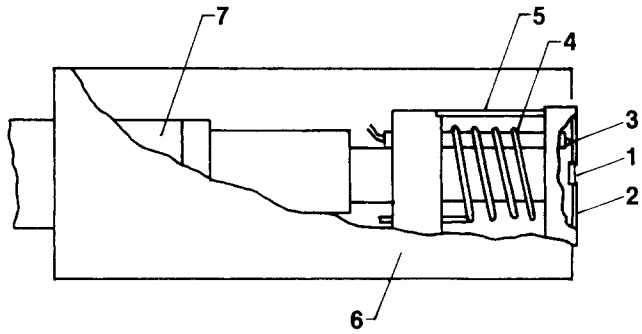

FIG. 3. A schematic of the GaAs crystal holder assembly showing (1) GaAs crystal, (2) Mo clamp, (3) thermocouple, (4) heating filament, (5) inner radiation shield, (6) outer radiation shield around whole assembly, and (7) the stainless steel tube which provides liquid nitrogen cooling.

II. THE GaAs PHOTOCATHODE

A. Apparatus

Cleaning, activating, and maintaining the GaAs photocathode requires ultrahigh vacuum, in the low 10^{-10} Torr range. The stainless steel vacuum chamber is built from a 10-cm diameter stainless steel cross and is pumped by a 30-l/s triode ion pump.

The GaAs sample holder is positioned by a manipulator which allows the GaAs to be retracted for activation (dashed lines in Fig. 1). The manipulator also has the capability for small lateral motions and tilt for positioning the GaAs in front of the electron optics assembly.[30] The electron optics is mounted independently on another 15-cm OD flange.

A schematic of the GaAs crystal holder assembly is shown in Fig. 3. The GaAs crystal (1) is clamped (2) against the Mo heater block which can be radiatively heated by the filament (4). (If Cu is used for the heater block, it will alloy with the GaAs and the GaAs crystal will melt at a temperature below the heat cleaning temperature.) The temperature is monitored by a thermocouple (3), spot-welded to the Mo block. Radiation shields (5) and (6) enclose the heater assembly. This assembly is attached to a thin wall stainless steel tube (7) that is electrically isolated from the manipulator flange by a ceramic break. The GaAs can be cooled by flowing liquid nitrogen into the stainless tube. Gentle pumping on a smaller central tube removes bubbles and

increases the cooling. Temperatures of 100–115 K at the Mo block are obtained after cooling for about ½ h.

The molecular beam cesium source used in activating the GaAs is similar to that described by Klein.[31] Cesium of 99.97% purity is purchased in glass ampules. We triply distill this Cs into smaller ampules at a pressure of $\sim 1 \times 10^{-8}$ Torr. One of these smaller ampules (~6 mm × 50 mm) is sealed in a Cu tube attached to a stainless steel valve.[31] After a bakeout with the valve open, the valve is closed and the Cs ampule is broken by squeezing the Cu tube. In operation, the Cu tube holding the Cs is held at ~80 °C and the valve at ~140 °C. At this temperature the Cs will not stick to the valve, and the Cs flow can be controlled. Just after breaking the ampule it is sometimes necessary to heat the Cu tube to a higher temperature (120–140 °C with the valve closed) to move the Cs out of the broken ampule. With the valve closed, the chamber can be opened to atmosphere and the GaAs crystal changed. Very little Cs is used in an activation, and such an ampule will last for over 100 activations.

Research grade oxygen (99.99% minimum purity) at 1 atm in a glass 1-l flask is attached to the chamber through a shutoff valve and a variable leak valve. A small tube directs the O_2 at the GaAs surface. In this way we minimize the amount of O_2 introduced and maintain an excess of Cs in the chamber; this affects the cathode lifetime as discussed in the activaton section below. On the other hand, it should be noted that, in some commercial photocathode processing, the O_2 is directed away from the cathode to improve uniformity.

B. GaAs material properties

Negative electron affinity GaAs photocathodes have been the subject of a large research and development effort since they were first reported by Scheer and van Laar in 1965.[32] It is not our purpose in this paper to review this field, but rather to report on our experience and emphasize details that could be especially important in polarized electron source applications. More information can be found in reviews of GaAs photocathodes.[33,34]

The (110), (100), (111)B, and (111)A faces of a p-type GaAs can be activated to negative electron affinity with best results for crystals doped in the range of 5×10^{18} cm^{-3} to 2×10^{19} cm^{-3}. The (110) surface is the cleavage plane. A polarized electron source using crystals cleaved in ultrahigh vacuum to obtain clean (110) surfaces has been reported by Erbudak and Reihl.[35] They found a polarization of only 21% for NEA (110) surfaces and therefore advocated operating in a positive electron affinity mode (PEA), as discussed below in Sec. III.

We have used (100) surfaces for which we find the polarization to be 43%. We use chemically polished (100) wafers[36] ~0.3 mm thick. Because the (110) cleavage planes are perpendicular to each other and to the (100) surface, it is easy to cleave the wafer into rectangular pieces of any desired size by pressing a knife edge at the edge of the wafer. The results obtained in this paper were obtained from (100) GaAs doped 5.6×10^{18} cm^{-3} p-type with Zn, with a resistivity of 0.0053 Ω cm and a mobility of 209 cm^2/V s.

No polarization measurements have been published to date for the (111) surfaces. The (111)B surface is easily chemically polished, has the highest photoelectron escape probability, and is often used for photocathodes.[37] However, (110) facets are formed on this surface at temperatures usually used for heat cleaning.[38] The presence of trace amounts of C on the surface, as is always present in surfaces exposed to the atmosphere, greatly increases the tendency to facet on heating.[39] Therefore, one might expect the polarization measurements of heat-cleaned (111)B surfaces to be similar to (110) surfaces. Faceting has also been reported[37] for (100) surfaces, but in general the (100) surface is much more stable against faceting.[40] Studies of unfaceted NEA (100) surfaces have been reported.[41,42]

So far we have discussed bulk material. Commercial photocathodes are usually made from epitaxially grown surfaces. These materials can be made cleaner and have longer diffusion lengths (up to 5 μm) which lead to higher quantum yields. We have activated a (100) surface grown by vapor phase epitaxy,[43] but at a time when we were not able to make polarization measurements. If spin relaxation of the photoelectrons (Sec. III) takes place primarily in the bulk, a longer diffusion length and hence a longer time in the crystal could lead to a lower polarization. If the depolarization mechanism is primarily a scattering at the surface,[18,35] then the larger yield of an epitaxially grown surface may be obtained without added depolarization.

More work is needed to optimize the GaAs source with respect to material properties (doping, epitaxial vs. bulk, etc.) and with respect to cleaning and activation as discussed below. Little data is currently available beacuse, once a source becomes operational, it finds immediate service in an experiment.

C. Cleaning the GaAs

The GaAs cleaning process has two stages: a chemical cleaning and further cleaning by heating in ultrahigh vacuum. It may be possible to eliminate the chemical cleaning by taking a crystal directly from epitaxial growth to the vacuum system for activation. For bulk wafers, a chemical cleaning is necessary. It has been shown, using Auger spectroscopy,[44] that the main contaminant on the GaAs after heating is carbon; care must be taken in the cleaning procedure to minimize carbon contamination.

The most widely used cleaning procedures employ an H_2SO_4, H_2O_2, H_2O etch with composition ratios in the range 5 : 1 : 1 to 3 : 1 : 1 or a Br-methanol etch of from ~0.5% to a few percent Br. The etching rate of the sulfuric acid solution as a function of concentration and temperature has been measured.[45] Etching times of 15 s to 5 min for the sulfuric acid etch and 0.5–2 min for the Br-methanol etch have been reported by different laboratories. There are many different cleaning procedures

with a variety of weights placed on the importance of different aspects of the procedure. The methods of preparing a GaAs substrate for epitaxial growth are different from methods of preparation for photocathode processing. The procedure reported here has been the most successful for us. It has been used without our analyzing whether each step is of crucial importance, and a condensed procedure may well prove adequate.

We use an etching procedure based on the work of Shiota, *et al.*,[46] which was brought to our attention by the SLAC group.[13] The detailed steps of the procedure are given in the Appendix. Attention to detail in the cleaning process is important. The amount of residual contamination depends on such details as, for example, the cleanliness of containers, water, and solvents and on length of the time and number of rinses.

After this chemical cleaning, the GaAs is mounted on the crystal holder, and the source chamber is pumped down as soon as possible. To achieve the ultrahigh vacuum necessary, the source chamber is baked for ~24 h at 180–220 °C. The bakeout may also be a source of contamination of the surface. Although our present source does not have such a feature, bakeout is sometimes avoided in cathode processing[37] by use of a high-vacuum interlock which allows insertion of the crystal after bakeout. During bakeout, we use the crystal heater to maintain the crystal temperature at ~300 °C.

The heat treatment to clean the surface is a crucial step in obtaining negative electron affinity. In the nonequilibrium (Langmuir) condition where the hot GaAs crystal is surrounded by the cold chamber walls, there is a range of temperatures where the Ga and As evaporate congruently, that is, together in equal proportions. Above the maximum congruent evaporation temperature, which has been measured as 657 °C[47] and 663 °C[48] for GaAs (100) (630 °C and 675 °C for (111)B and (111)A, respectively[48]), the As evaporates preferentially as As_2, leaving behind small Ga droplets on the surface.

There are a wide range of "best" temperatures for heat treatment reported in the literature. Generally the temperatures are not easily measured. The disadvantage of using an IR pyrometer to measure the temperature is that the emissivity is a poorly known quantity. Measurements with a nearby thermocouple give the temperature of the structure holding the crystal rather than that of the crystal. The temperatures we report in this paper are those of the Mo piece against which the crystal is pressed. Thus, the proper temperature for heat cleaning must be found from experience with each apparatus. Once found, as long as it can be measured reproducibly, its absolute value is not of concern. One way to find this temperature is to sacrifice a crystal. By heating to successively higher temperatures and looking at the cooled surface with obliquely incident light between each heating, there will be a point where the surface appears frosty. This is the temperature at which Ga droplets form. Heating to a temperature that produces a very slight frostiness, or to temperatures 10–20° lower than this, produces good cathodes.

The time for which the crystal is heated also varies widely as reported in the literature. We heat our crystals to 640 °C for 5 min and then to 650 °C for 1–2 min. We have heated to temperatures as high as 700 °C, which we believe were required because of poor thermal contact between the crystal and the Mo block. Some workers favor the high–low technique,[41,49,50] where the first heat cleaning and activation are followed by a second activation after heating a second time to a lower temperature.

The base pressure in our chamber is in the low 10^{-10} Torr range. During the first heat cleaning of the crystal, the pressure may rise into the high 10^{-8} Torr range. On subsequent heat cleanings the pressure rises into the low 10^{-9} Torr range and is back in the 10^{-10} Torr range within 5 min after the heating is stopped. We observe a possible cleaning effect due to the reactivation process itself in that subsequent activations of a crystal are usually better than the first. Piaget[50] has found that surface carbon contamination is reduced by reaction with oxygen at the high temperatures present when an activated cathode is heat-cleaned.

Argon ion bombardment has also been used to clean the GaAs surfaces.[42] While carbon contamination can be removed by ion bombardment, defects are introduced which decrease the photoemission sensitivity of the photocathode.[41,50] Ion bombardment is therefore to be avoided. Auger spectroscopy can be a useful diagnostic tool in developing cathode preparation methods, but the Auger spectrometer can also be a source of contamination. Furthermore, the electron beam can crack hydrocarbons on the GaAs surface leaving C contamination, unless the GaAs is heat-cleaned before the electron beam is applied.[41]

D. Activation

After heat cleaning the GaAs as described above, it is cooled in ~10 min to 30 °C. To save time, we use liquid nitrogen cooling for a short period. Activation is done in the 20–30 °C temperature range. If the crystal becomes too cold, it is warmed with the heater.

For activation, the crystal is in the retracted position about 3 cm from the aperture which is biased at +100 V to collect the photoelectrons. The mlm standard white light source is focused on the crystal, and activation is started by opening the Cs valve. Within about 5 min photocurrent is observed. A peak in the photocurrent is reached at a sensitivity of 15–40 μA/lm. At this point O_2 is leaked in, and Cs and O_2 are deposited simultaneously so as to maximize the rate of increase of the photocurrent. The sensitivity increases within about 5 min to 300–600 μA/lm, a which point it reaches a maximum, and it becomes difficult to maintain the Cs and O_2 balance. We try to maintain the sensitivity constant for another 5–10 min before shutting off the Cs and O_2. Since our chamber tends to be Cs deficient, we usually overcesiate slightly at the end of this procedure, which temporarily decreases the sensitivity by 10–20%.

A typical activation is shown in Fig. 4, where the

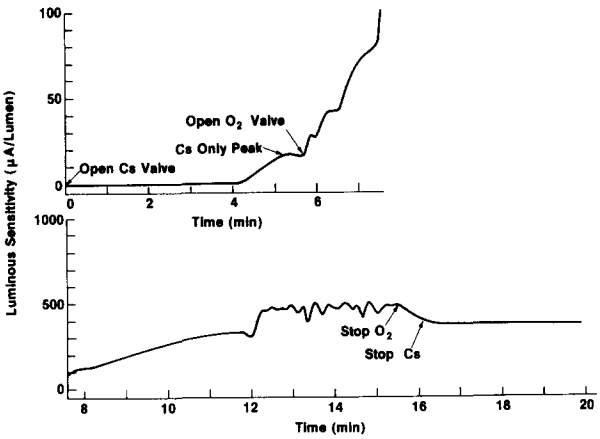

FIG. 4. The luminous sensitivity as a function of time is shown for a typical activation. (Note the luminous sensitivity scale change from the upper to lower part of the figure.)

photocurrent is plotted as a function of time. The zero is established by blocking the light as there may be some leakage current. After 4 min the photocurrent is observed to increase and reaches a Cs only peak of 17 μA/lm. If the photocurrent is monitored initially on a more sensitive electrometer range, a dramatic increase in the photocurrent of several orders of magnitude is observed. During co-deposition of Cs and O_2 we aim for a smooth increase in photocurrent, but, as is evident from Fig. 4, the O_2 cannot always be controlled precisely enough to achieve this. For example, the dip at 12 min is a result of the mixture having become Cs rich; when the O_2 flow is increased, there is a significant increase in photocurrent. The excess Cs at the end of deposition decreased the sensitivity, but it increased again as the cathode aged and came to equilibrium. Acceptable cathodes can be obtained even when there are considerable deviations from the optimum Cs and O_2 flow. We have, however, killed a cathode by applying too much O_2; it was necessary to heat-clean again and reactivate.

The simultaneous deposition method is used because we find it fast and convenient. We have obtained similar results by applying Cs and O_2 alternately. The Cs is applied until the first photocurrent maximum is obtained. Then O_2 is applied to decrease the photocurrent to 20–50% of this value. If there is slight excess of Cs in the initial maximum, the photocurrent will increase before it decreases with O_2. Then Cs is applied again to bring the photocurrent back up to a new maximum. This is repeated several times until no further increase is observed.

Another check on the photocathode, in addition to measuring its luminous sensitivity, is to measure the ratio of white light photocurrent to the photocurrent with the red filter (RG715)[20] in place. This ratio is typically 2 or less.

The behavior of the photocathode after activation depends in large part on the Cs–O balance in the chamber. In commercial phototubes there is an excess of Cs to maintain a partial pressure of Cs in the tube. We find that in a freshly baked ultrahigh vacuum chamber our photocathodes become Cs deficient quite rapidly. Fortunately, this can be corrected by opening the Cs valve and "peaking up" with Cs. This may be done with the crystal in operating position; line of sight is not required as some Cs moves around the chamber at room temperature. The cathode should be at room temperature for peaking up; with the cathode at liquid nitrogen temperature, poor results are obtained, presumably due to the lower mobility of the Cs on the cathode surface. A fresh vacuum chamber becomes "seasoned" after a few activations or peaking up with Cs.

The quantum yield of one of our photocathodes is shown in Fig. 5. The threshold of the yield measured at 110 K is ~0.8 eV higher in energy than at 300 K, due to the increase of the band gap at the lower temperature. The overall yield at 110 K is also slightly lower than at room temperature. We have also observed cathodes where the yield (in the flat region of the curve) increased on cooling; we believe these differences in behavior are related to the Cs balance in the chamber. The yield curves have the sharp knee at threshold characteristic of a negative-electron affinity. The yield is about a factor of 2 lower than the best we have achieved and about a factor of 8 less than typical commercial cathodes. We attribute this to the starting materials, possible deficiencies in the cleaning procedure, and lack of perseverance once satisfactory cathodes for a source of spin-polarized electrons were achieved.

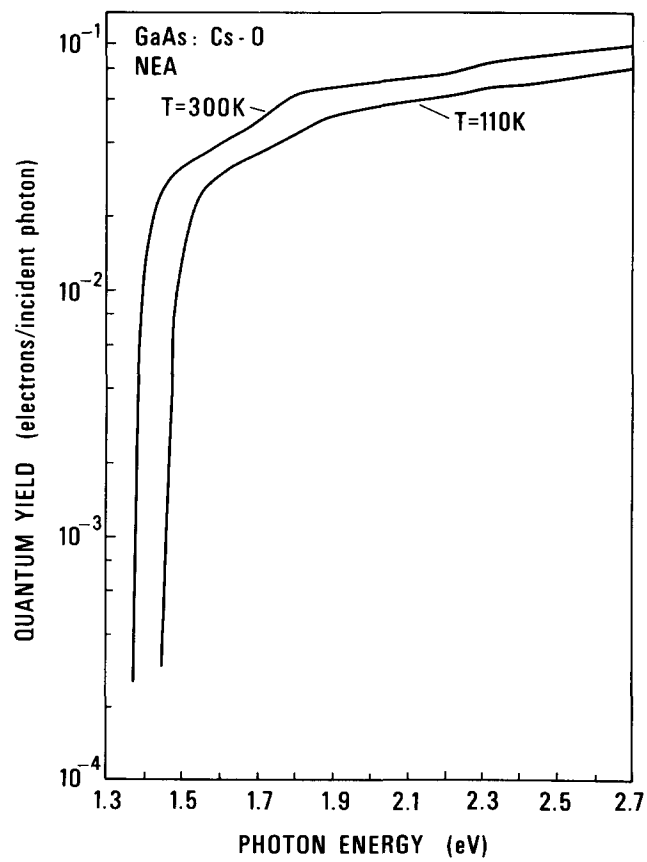

FIG. 5. The quantum yield curves of one of our photocathodes measured at temperatures of 110 K and 300 K are shown. The sharp knee at threshold is characteristic of a negative electron affinity.

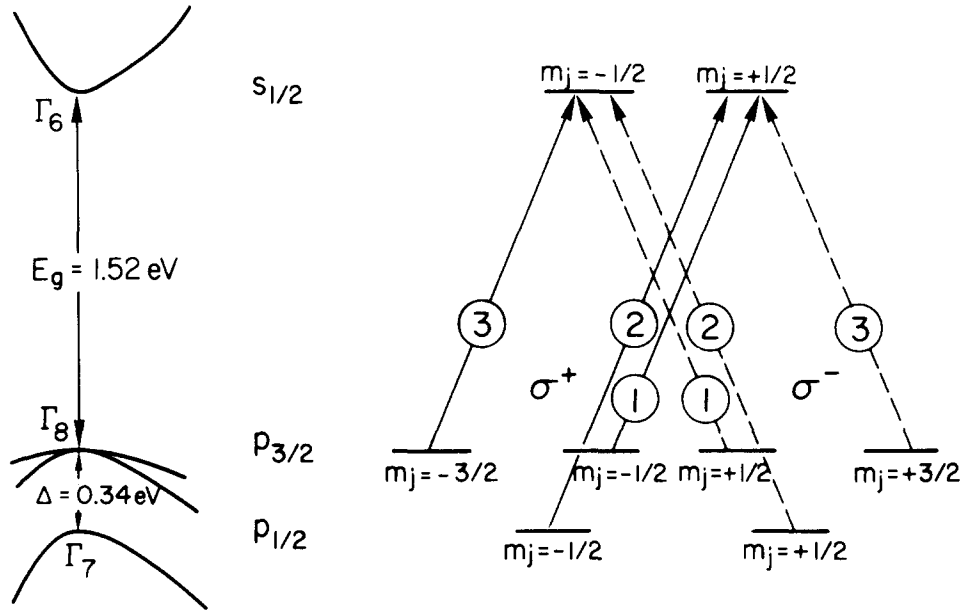

FIG. 6. The energy bands of GaAs near the center of the Brillouin zone (Γ point) are shown at the left of the figure. The band gap is 1.52 eV and the spin–orbit splitting of the valence bands is 0.34 eV. On the right, the allowed transitions between m_j sublevels for circularly polarized light, σ^+ (solid lines) and σ^- (dashed lines), are shown. The circled numbers give the relative intensities; thus the $p_{3/2} \rightarrow s_{1/2}$ transition with one helicity light gives three times as many excited electrons of one spin as of the other spin. Changing the helicity of the light reverses the spin direction of the excited electrons.

III. PHOTOEMISSION OF SPIN POLARIZED ELECTRONS

The three-step model of the photoemission process,[51] photoexcitation, transport to the surface, and escape into vacuum, is applicable to photoemission from NEA GaAs.[34] A detailed discussion of how the spin polarization of the electrons is created in the photoemission process is given in Ref. 11 and will be summarized here very briefly. The electron transport and emission process will be reviewed, as will possible concurrent depolarization processes. Finally, spin polarization and yield measurements are presented for NEA and PEA surfaces.

A. Polarization by photoexcitation

A key factor in obtaining polarized electrons is the spin–orbit splitting of the valence bands of GsAs which is shown in Fig. 6. At the Γ point, the valence band maximum, the otherwise degenerate p band is split into a fourfold degenerate $p_{3/2}$ level and twofold degenerate $p_{1/2}$ level, which is located 0.34 eV lower in energy. The origin of the spin polarization can be understood by considering the transitions from the m_j sublevels shown on the right-hand side of Fig. 6. For circularly polarized light, the optical selection rules require that $\Delta m_j = +1$ for σ^+ or positive helicity light (solid lines in Fig. 6) and $\Delta m_j = -1$ for σ^- light (dashed lines in Fig. 6). The quantization axis is defined by the light angular momentum direction.

The relative transition probabilities are readily calculated[11] and are shown in circles on Fig. 6. For σ^+ light, three times as many electrons go to the $m_j = -\frac{1}{2}$ as to the $m_j = +\frac{1}{2}$ state. The spin polarization is

$$P = (n\uparrow - n\downarrow)/(n\uparrow + n\downarrow) \qquad (1)$$

where $n\uparrow$ and $n\downarrow$ are the numbers of electrons with spins parallel and antiparallel to the light direction respectively. Thus for σ^+ light we have $P = -50\%$ and for σ^- light $P = +50\%$. When electrons are also excited from the spin–orbit-split-off band at Γ_7, the polarization goes to zero.[11] The maximum polarization is obtained for photon energies less than 0.1 eV greater than the band gap energy.

A very important feature of this process for a polarized electron source is the ease of polarization reversal. The circular polarization of the incident irradiation can be changed external to the system as described in Sec. I. No parameter of the electron beam is changed by going from σ^+ to σ^- light except the spin polarization direction. In particular, the intensity remains constant as the spin polarization is modulated.

B. Transport and emission

As we have described in some detail, GaAs has the property that it can be activated to form a negative electron affinity photocathode. As is apparent from Fig. 7(a), it is really an effective negative electron affinity; even though the vacuum level is below the conduction band minimum in the bulk, it is not below the conduction band minimum at the surface. Throughout this paper we have adopted the conventional terminology and do not use the qualifier "effective." The important factor is that electrons at the energy of the bulk conduction band minimum have no potential barrier impeding their escape into the vacuum.

The electrons are excited in a region determined by the light absorption length α^{-1}, where $\alpha^{-1} \sim 1\ \mu$m. The electrons thermalize to the conduction band minimum in $\sim 10^{-12}$ s, where they can diffuse to the surface and be emitted.[52] The emission is limited by the electron diffusion length L and, once the electrons get to the surface by the escape probability, P_{esc}. The diffusion length ranges from $\sim 0.5\ \mu$m for bulk material to several micrometers for epitaxially grown material; this leads to a very high quantum yield.

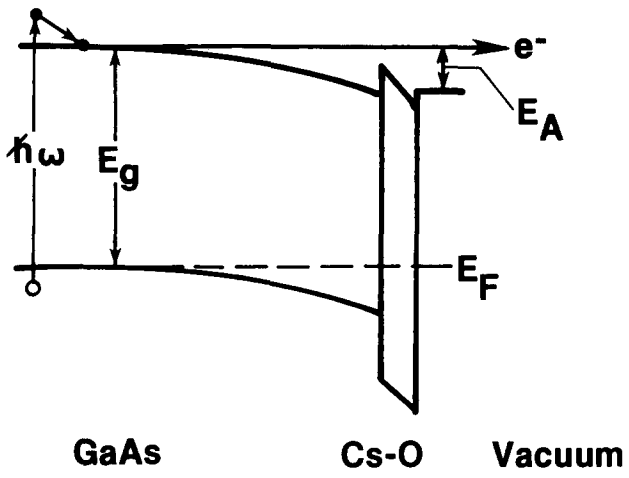

(a)

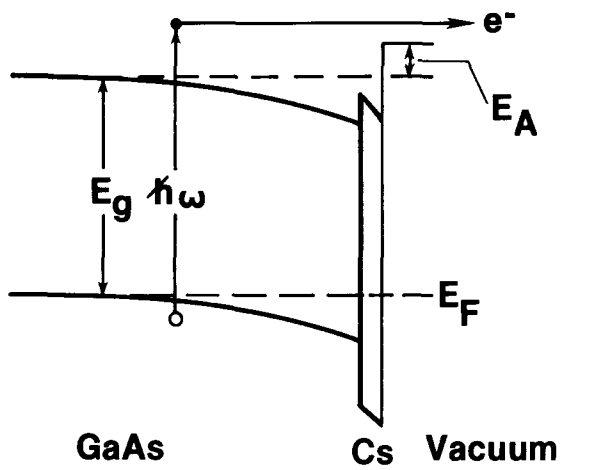

(b)

FIG. 7. The valence and conduction bands of p-type GaAs bend downwards in energy at the surface. A negative electron affinity (vacuum level lower than the bulk conduction band minimum) is obtained by activation with Cs and O_2 as shown in (a). Electrons excited across the band gap E_g by photons of energy $\hbar\omega$, thermalize to the conduction band minimum, and diffuse to the surface to escape into the vacuum. Very high quantum yields can be achieved. Activation with Cs alone can produce a small barrier at the surface giving a positive electron affinity as shown in (b). The quantum yield at threshold is lower because an electron can lose energy by scattering with phonons, such that it falls below the barrier.

In contrast, clean GaAs has an electron affinity of about 4 eV. The depth of the region from which the electrons escape is determined by the mean free path for electron–electron scattering and is of the order of 10 Å. When there is a small positive affinity of a few tenths of an eV as shown in Fig. 7(b), the escape depth is limited by electron-phonon scattering and is of the order of 100 Å.[34]

The quantum yield Y for an NEA cathode can be described by the equation[52]

$$Y = P_{esc}/[1 + (\alpha L)^{-1}]. \quad (2)$$

This equation is valid in the photon energy range from the band gap energy E_g to $E_g + 0.3$ eV, where one can take the fraction of electrons thermalizing to the Γ minimum to be unity and the fraction of electrons thermalizing to the X or L minima to be zero. The escape probability P_{esc} is determined by the probability of transmission at the surface potential, the probability of reflected electrons getting another chance at escape, and by the surface recombination probability. From Eq. (2) it can be seen that P_{esc} determines the magnitude of the yield curves while L determines their shape.

We now consider the energy distribution of the emitted electron beam. The peak in the energy distribution of thermalized electrons in the bulk of the crystal at 100 K is about 5 meV above the Γ minimum. In the band bending region, however, these electrons become hot electrons. As discussed by James and Moll,[52] scattering can take place to X and L minima giving rise to a lifetime broadening. Electrons can also lose energy to optical phonons in the approximately 80 Å wide[37] band bending region; the probability of gaining energy at liquid nitrogen temperature is very small. This leads to an asymmetric peak with a low energy tail. We measured such a distribution with a FWHM of 0.13 eV as discussed in Sec. IV.

The angular spread of the photoemitted electrons is also determined by the details of the emission process as has been discussed by Bell.[33] The electron wave vector parallel to the surface is conserved on emission within a reciprocal lattice vector **g**, which must be zero for the low energies of interest here. If the tangential kinetic energy inside the surface is $\frac{1}{2}kT$, then outside it is $\frac{1}{2}kT(m^*/m)$, where m^* is the electron effective mass in the crystal. The kinetic energy normal to the surface in the vacuum is the difference between the conduction band minimum E_c and the vacuum level E_∞ which is about 0.2 eV. Thus, Bell calculates the cone half-angle of the emitted electrons[33]

$$\theta \approx \tan\theta = [\tfrac{1}{2}kT(m^*/m)/(E_c - E_\infty)]^{1/2} \quad (3)$$

to be 4° at room temperature. In the photoemitted electron beam there is actually a distribution of kinetic energies and the angular distribution is a function of the energy. Pollard[53] measured a cone half-angle of 5°. However, this measurement has been criticized by Bradley *et al.*,[54] who measure an external transverse kinetic energy of 107 ± 18 meV corresponding to a cone half-angle of approximately 30°. Even though locally the electron emission may obey Bell's model, real surfaces are not perfectly flat. Surface polishing or etching, and Ga droplets or facets formed on heat cleaning all could contribute to a surface roughness that would broaden the actual angular distribution.

C. Depolarization

The depolarization of electrons photoexcited to the conduction band minimum has been widely studied by measurements of the recombination luminescence.[55] By measuring the circular polarization of the luminescence as a function of magnetic field, it is possible to determine the electron lifetime τ and the spin relaxation time τ_s at the bottom of the conduction band. Fishman and Lampel[56] have analyzed depolarization mechanisms and

conclude that, for GaAs up to temperatures of the order of 100 K, τ_s is determined by the exchange interaction between the electrons and holes as suggested by Bir, Aronov, and Pikus.[57] Other measurements have been interpreted[58] in terms of the D'yakonov–Perel'[59] mechanism where the depolarization is a band structure effect related to the spin–orbit splitting and lack of inversion symmetry. The polarization of the excited electrons P_L determined by luminescence measurements is less than the theoretical polarization P_{th} as given by the equation

$$P_L = P_{\text{th}}\tau_s/(\tau + \tau_s). \tag{4}$$

The electron lifetime τ is material dependent and is influenced by deep levels (defects, impurities, etc.) that act as recombination centers.

An equation analogous to Eq. (4) was postulated for the photoemission case in Ref. 11, where the lifetime τ was replaced by some average photoemission time. This approximation is not strictly correct, and in order to make a quantitative comparison between the polarization of photoelectrons and the luminescence polarization, the details of the photoemission process, such as the finite penetration of the light and the diffusion of the excited electrons to the surface, must also be considered. We do this using a one-dimensional diffusion model as described by Bell.[33] Equation 3.4 of Ref. 33 can be generalized to two equations for the up spin density $n_\uparrow(x)$ and down spin density $n_\downarrow(x)$ in equilibrium

$$\frac{\partial n_\uparrow}{\partial t} = D(\partial^2 n_\uparrow/\partial x^2) - n_\uparrow(x)/\tau - \tfrac{1}{2}(n_\uparrow - n_\downarrow)/\tau_s + G_\uparrow(x) = 0, \tag{5a}$$

$$\frac{\partial n_\downarrow}{\partial t} = D(\partial^2 n_\downarrow/\partial x^2) - n_\downarrow(x)/\tau - \tfrac{1}{2}(n_\downarrow - n_\uparrow)/\tau_s + G_\downarrow(x) = 0. \tag{5b}$$

D is the electron diffusion coefficient and x is the direction normal to the surface. The minority carrier lifetime τ and spin relaxation time τ_s are the same as in Eq. (4). We are neglecting, for the moment, any extra depolarization in the band bending region or activation layer. The generation of electrons is described by $G(x)$.

$$G_\uparrow(x) \propto C_\uparrow e^{-\alpha x}, \tag{6}$$

where $C_\uparrow$ is the matrix element for generating up spin electrons and α is the absorption coefficient for the incident light. There is an analogous equation for $G_\downarrow(x)$. Writing $n^+ = n_\uparrow(x) + n_\downarrow(x)$, $n^- = n_\uparrow(x) - n_\downarrow(x)$, and $G^\pm = G_\uparrow(x) \pm G_\downarrow(x)$, we obtain on adding and subtracting (5a) and (5b),

$$D(\partial^2 n^+/\partial x^2) - n^+/\tau + G^+ = 0, \tag{7a}$$

$$D(\partial^2 n^-/\partial x^2) - n^-/T + G^- = 0, \tag{7b}$$

where $T = \tau_s\tau/(\tau_s + \tau)$. Equations (7a) and (7b) are now of the form solved by Bell, which for one-dimensional diffusion in a thick solid gives the current at the surface, $x = 0$, due to generation at x (Eq. 3.46 of Ref. 33),

$$\frac{dJ(0)}{dx} = \frac{S}{S + (D/L)} G(x) \exp(-x/L). \tag{8}$$

In Eq. (8), S is the total surface recombination velocity. Using Eq. (6), we can integrate Eq. (8) for the "currents" $J^+(0)$ and $J^-(0)$ of n^+ and n^- reaching the surface. Assuming P_{esc}, the fraction of the current which escapes into vacuum, is spin independent, the polarization of the photoemitted electrons is

$$P = \frac{J^-(0)}{J^+(0)} = \frac{(S + D/L)(\alpha + 1/L)}{(S + D/l)(\alpha + 1/l)} P_{\text{th}}, \tag{9}$$

where $P_{\text{th}} = (C_\uparrow - C_\downarrow)/(C_\uparrow + C_\downarrow)$, the minority carrier diffusion length $L = \sqrt{D\tau}$, and the "spin asymmetry diffusion length" $l = \sqrt{DT}$. As discussed by Bell,[33] a good approximation for GaAs is that $S \gg D/L$ and $S \gg D/l$. Then, Eq. (9) simplifies to

$$P = [\alpha + (D\tau)^{-1/2}][\alpha + (DT)^{-1/2}]^{-1} P_{\text{th}}. \tag{10}$$

The photon energy of the light we use is just above threshold where $\alpha \sim 1\ \mu\text{m}^{-1}$.[60] As shown below in Sec. IIID, the diffusion length of our cathodes is ~0.5 μm so that $(D\tau)^{-1/2}$ is about twice α. We see from Eqs. (4) and (10) that the spin polarization of photoemitted electrons is larger than the luminescence polarization. For example, if the luminescence polarization is 30%, then for $(D\tau)^{-1/2} = 2\alpha$ the polarization of the photoelectrons is expected to be 42% from Eq. (10).

From luminescence measurements it is known that τ is approximately temperature independent but that τ_s decreases with increasing temperature. We have measured the temperature dependence of the spin polarization from our (100) GaAs photocathodes. The polarization at 110 K is 1.2 times that at 300 K. Since in the present apparatus it takes nearly half an hour to cool to 110 K, and the polarization at room temperature is sufficient for many measurements, we sometimes operate the photocathode at room temperature, especially when setting up an experiment.

There may be additional depolarization in the band bending region and activation layer. For hot electrons in the band-bending region the spin relaxation time has been observed in luminescence measurements at liquid nitrogen temperature to be less than in the bulk.[61] There is also the possibility of the photoelectrons undergoing spin exchange scattering in the Cs–O layer. The cross section for spin exchange scattering from alkali atoms at low energies is very large.[62] The activation layer is known to be on the Cs-rich side of Cs_2O.[34] Some atomic-like Cs could be present, providing a large source of depolarization. Possible evidence for this has been observed in photoemission from NEA GaAs (110)[35] and PEA GaAs (110).[11]

D. Polarized photoemission from NEA surfaces

We have measured the polarization of photoelectrons from the NEA (100) GaAs photocathodes indirectly by making polarized LEED measurements[14] at a W(100)

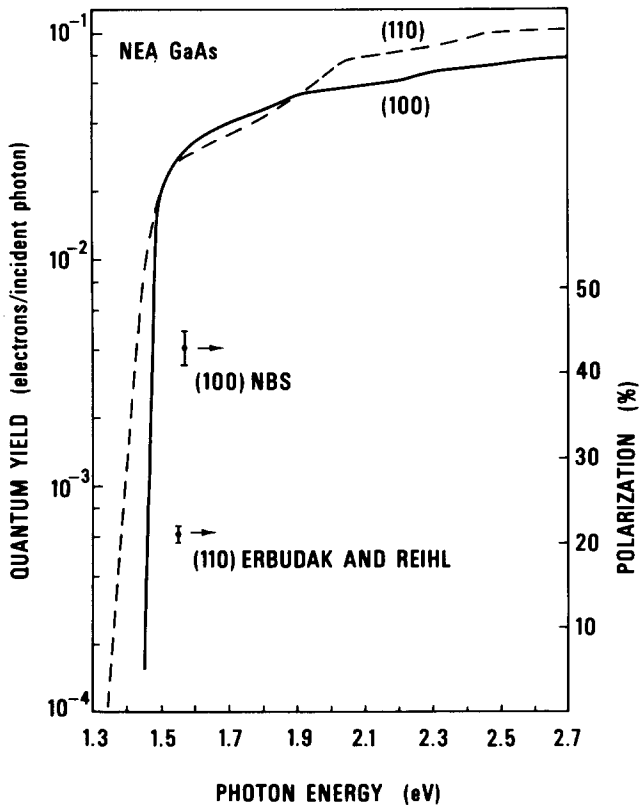

FIG. 8. The quantum yield curves of a heat-cleaned GaAs(100) surface and a vacuum-cleaved (110) surface (Ref. 35) measured at 110 K and 77 K are compared (left ordinate). The yield is quite similar for both faces, but the spin polarization at threshold (right ordinate) is very different.

surface. We were able to compare our measurements of the specular scattering (00 beam) at angles of incidence from 10° to 17° to equivalent[14] measurements of Kalisvaart, *et al.*[63], who used a Mott detector to measure the spin polarization. The polarization of our source was determined by using the polarization, $P = 43\%$, that produced the best agreement between our curve at some angle of incidence, such as 13°, and the curve of Kalisvaart, *et al.* The uncertainty in this polarization determination of $\pm 2\%$ was estimated by comparisons between data at other angles of incidence. The polarization was measured with the photocathode at 110 K and at the photon energy, $\hbar\omega = 1.57$ eV, of the GaAlAs diode laser. In Fig. 8 the polarization measurement is shown (refer to right axis) along with the quantum yield (refer to the left axis).

Also shown in Fig. 8 are recent measurements of Erbudak and Reihl[35] of NEA (110) surfaces. They found a maximum polarization of 21% at $\hbar\omega = 1.55$ eV with little variation over the photon energy range 1.50 eV $< \hbar\omega <$ 1.60 eV at a measurement temperature of 77 K. This result led them to conclude that NEA and a high polarization exclude each other and that it is undesirable to operate in an NEA mode. Figure 8 makes very clear that their conclusion does not apply in general. [An earlier investigation[11] of GaAs (110) reported a high polarization (~40%) and NEA. From the reported yield curve, it is now apparent that the electron affinity in these early measurements was zero or slightly positive, consistent with the results of Erbudak and Reihl.[35]]

It is curious that although the yield curves from the two faces are so similar, the polarization is strikingly different. Possible origins of this difference have been discussed in a recent paper.[18] The (100) and (110) GaAs cathodes were doped p-type at 5.6×10^{18} cm^{-3} and 1×10^{19} cm^{-3}, respectively. The (100) GaAs was heat-cleaned, as described in Sec. II, whereas the (110) GaAs surfaces were obtained by cleaving in vacuum. The activation at room temperature with Cs and O_2 appears to be similar in both cases. The difference in P could be caused by differences in τ and τ_s from one face to the other. The similarity of the yield curve indicates that the diffusion length, and hence τ, is about the same in each case. Erbudak and Reihl attribute the depolarization to spin exchange scattering. An attractive explanation of how the depolarization might be so different on the two faces is to be found in the details of the photoemission process as calculated by Burt and Inkson[64] and discussed in Ref. 18. In brief, the anisotropy of the wavefunctions at the Γ minimum causes the transmission coefficient and the surface recombination velocity at the (110) surface to be much less than at the (100) surface. This leads to a model of the emission for the (110) face where an electron makes repeated attempts at transmission into the vacuum. It travels to the surface, gets reflected at the large potential step at the Cs–O/vacuum

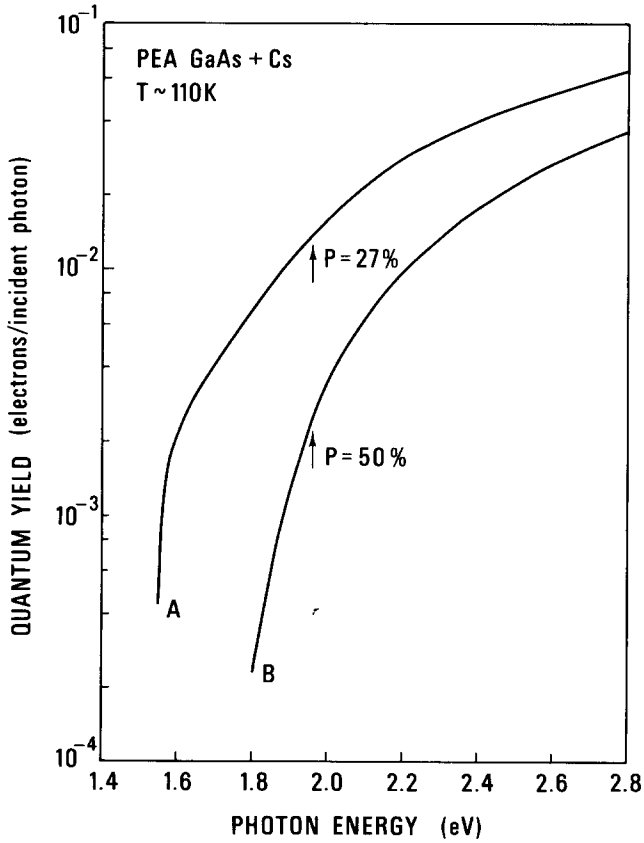

FIG. 9. The quantum yield is shown for two positive electron affinity GaAs(100) cathodes activated with Cs only. The photothreshold is about 1.6 and 1.8 eV for curves A and B, respectively. The polarization measured at $\hbar\omega = 1.95$ eV is indicated.

interface, and then gets turned around again in the band-bending region for another attempt at escape. At the (100) face, on the other hand, an electron is very likely to recombine if it is not transmitted; multiple escape attempts are not likely. The depolarization due to spin exchange scattering could be much greater on the (110) face because electrons pass through the activation layer many times as they attempt to escape from the surface.

The escape probability P_{esc} and the diffusion length L can be determined by analyzing the yield of Fig. 8 using Eq. (2). Rewriting Eq. (2),

$$\frac{1}{Y} = \frac{1}{LP_{esc}\alpha} + \frac{1}{P_{esc}}, \tag{11}$$

and plotting Y^{-1} against α^{-1}, we obtain P_{esc} from the intercept and L from the slope. It is, of course, necessary to know α independently.[60,65] The accuracy of this procedure depends on the accuracy with which α, which depends on doping, is known. To analyze our low temperature yield, we made a 0.75-eV rigid shift of the room temperature absorption data corresponding to the temperature shift of the absorption edge. We found $L = 0.4$ μm and $P_{esc} \simeq 0.1$.

A suitable figure of merit describing a photocathode as a spin polarized electron source is P^2Y. This removes the arbitrariness of the light source from the figure of merit P^2I discussed in the Introduction. The yield and polarization measurement for the (100) surface in Fig. 8 give $P^2Y \simeq 6 \times 10^{-3}$.

E. Polarized photoemission from PEA surfaces

If only Cs is applied in the activation process, a positive electron affinity surface as shown in Fig. 7(b) can be obtained. The threshold is a function of Cs coverage. We did not make a thorough investigation of PEA cathodes. In our preliminary experiments, we found that the photothreshold was not stable.

Two yield curves from PEA emitters are shown in Fig. 9. The photothresholds of curves A and B are about 1.6 and 1.8 eV, respectively. The polarization was measured at $\hbar\omega = 1.95$ eV, using a He–Ne laser light source. The polarization for cathode B was measured near threshold and a high $P = 50\%$ was found. Polarization greater than 50% is possible and has been observed for PEA emitters.[11] The polarization can be increased above 50% because the emission is restricted by the PEA to be near a direction in k space determined by the surface normal. For curve A in Fig. 9, the polarization is significantly lower because the photoexcitation takes place well above threshold. An increase in polarization is possible with a PEA emitter with a sacrifice of the yield.

Reihl, *et al.*[66] have used PEA GaAs (110) to overcome the low polarization observed for the NEA (110) surface. With PEA, the electrons are emitted primarily from the L minimum which lies 0.3 eV higher in energy than the Γ minimum. The absence of the peculiarities of emission at NEA (110) and the higher kinetic energy of the emitted electrons lead to a decreased spin exchange scattering. Reihl, *et al.* have found $P = 35\%$ at $\hbar\omega = 1.95$ eV and have achieved a figure of merit $P^2Y \simeq 1 \times 10^{-3}$.

IV. ELECTRON OPTICAL DESIGN

A. Overview

Most of the description thus far of the GaAs polarized electron source has been quite general without regard to a particular application. In this discussion of electron optical design, we illustrate how one matches the general electron optical characteristics of the GaAs photocathode to a particular experiment, in this case polarized low-energy electron diffraction.

The transversely polarized electron beam required for the PLEED experiment is produced from the initial longitudinal polarization by the 90° spherical deflector which changes the electron's momentum direction without affecting its polarization direction. A series of lenses accelerates the beam for transport through the isolation valve at an energy of 1000 eV with the consequence that the beam can be transmitted through small apertures. This allows for the possibility of efficiently using differential pumping to dynamically isolate the photocathode from possible high gas pressures in the target region. The high transport energy also minimizes the effect of stray magnetic fields. The source can be completely isolated from the experimental chamber by a large straight-through ultrahigh vacuum valve. This permits the GaAs cathode to remain activated while the main scattering chamber is opened to the atmosphere.

It is convenient that the target crystal of the PLEED experiment be at ground potential. All elements of the gun were therefore designed to be capable of floating at the required voltages relative to the cathode potential, which determines the electron beam energy at the target crystal. The source is modular in the sense that it is compact and could be decoupled at the valve. The beam characteristics at that point are suitable for matching to many other types of experiments.

After the valve the polarized electron beam from the source enters the LEED gun, which forms a suitable beam for the diffraction experiment. For our purpose, the polarized electron gun was to be a direct mechanical replacement in a commercially available[67] LEED apparatus. The LEED gun should meet several requirements. Since the bulk of LEED data is taken by scanning the energy of the incident beam, the spot size and focal point should remain stable as the beam energy is varied. The LEED gun should focus the beam to a spot size less than 1-mm diameter at about 10 cm from the end of the gun with a convergence half-angle of less than 0.5° at the target. The LEED gun should have an energy range of from a few eV to at least 250 eV.

B. Theory and calculation

1. Characteristics of the emitted beam

While the desired beam characteristics in terms of beam size, divergence, or both, at the target, are well

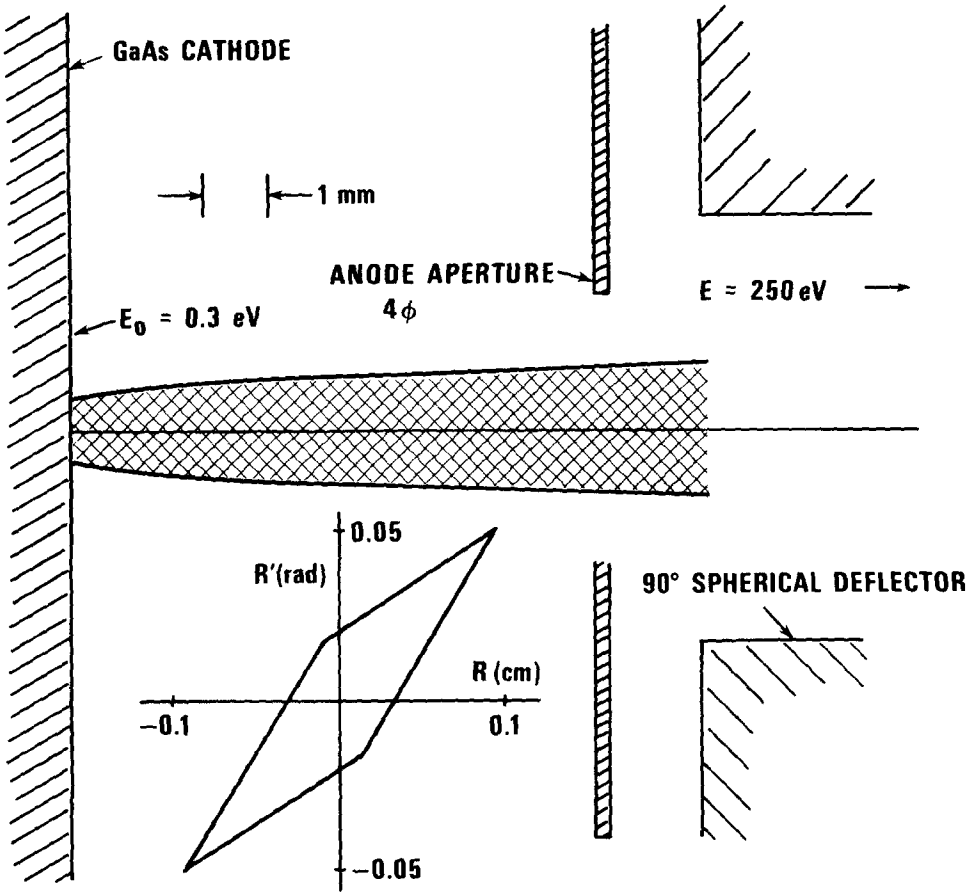

FIG. 10. The schematic shows the detail of the cathode region including the calculated electron beam envelope for $E_0 = 0.3$ eV. The emittance diagram of the beam at a kinetic energy of 250 eV, where R' is the slope of the trajectory and R is the radius, is inserted at the bottom of the figure.

defined, the characteristics of the emitted beam are usually not as well known, and it is difficult to measure the beam parameters necessary as input for an electron optical design. The emitted beam parameters needed for a realistic beam transport calculation are: the beam size, the energy distribution, and the angular distribution as a function of energy.

In our present case, the only parameter known with certainty is the emitted beam size, clearly defined by the size of the incident photon beam. In some preliminary design calculations we assumed an angular divergence of $\pm 5°$ on the basis of measurements[53] which seemed to indicate a strongly directed beam at the emitting GaAs surface. Later information[54] and our experimental observations indicated that this estimate was low. The design calculations were repeated using a conservative estimate for the half-angle of divergence of 40°. This particular assumption may have resulted in an overdesign factor, as the true divergence may be somewhat less.

As input to the beam transport calculations, we began by using an approximate energy distribution at the source based upon the measurements of James and Moll[52] and later refined the calculations using our own measurements of the energy distribution. In this calculation we represent the energy distribution by four discrete energies distributed in the following manner: 27.6% at 0.35 eV, 45.4% at 0.25 eV, 21.6% at 0.15 eV, and 5.4% at 0.05 eV. For a quantitative beam transport calculation through the system where the amount of beam transmitted through some restricting geometry is to be obtained, one must follow each of the current components separately throughout the system. This point will be illustrated later on when the incident beam is matched to the LEED gun acceptance.

2. Design of the cathode region

In order to maximize the angular aperture for the incident light, we wanted to minimize the distance between the GaAs photocathode and the 90° spherical deflector which contained a defining aperture for the light. A simple diode geometry was chosen as shown in Fig. 10. The photoelectrons are accelerated in an approximately uniform field to an aperture in the anode at a potential of 250 V. No other elements were placed between the GaAs and the 90° spherical deflector; an f/10 acceptance for the light incident on the GaAs crystal was obtained.

The pass energy of 250 eV for the 90° spherical deflector was chosen to minimize dispersion and maximize the transmission of the electron beam. The object and image focal points of the 90° spherical deflector are at the entrance and exit planes, respectively.[68] An incident parallel beam would cross over at the image focal point at the exit plane, and a point source or object at the entrance would be translated into a parallel beam at the exit. The property of the $1/r^2$ field is such that to a first approximation the beam is focused stigmatically in the plane perpendicular to the direction of beam propagation.

Our calculations in the cathode region show that the

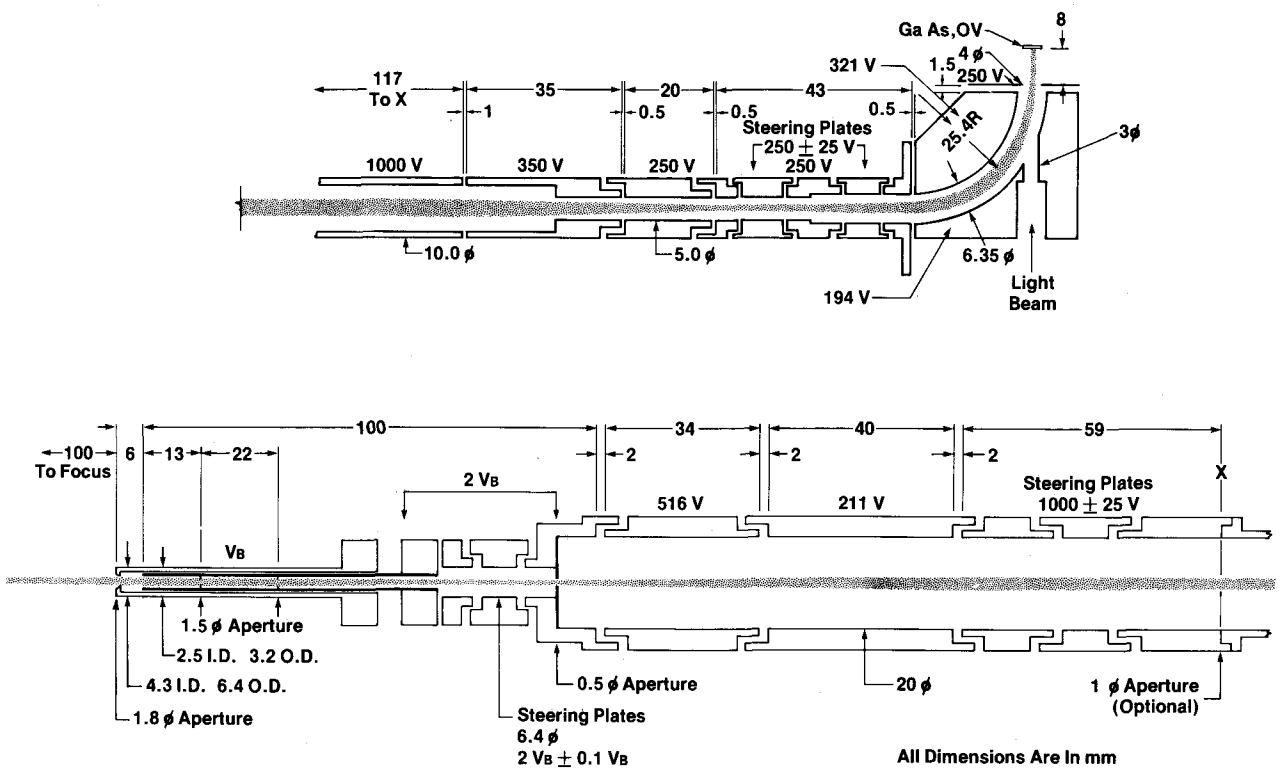

FIG. 11. A detailed schematic of the electron optics from the photocathode to the target showing the calculated beam envelope. The upper part of the figure can be considered the "source" and takes electrons up to the isolation valve. The lower part of the figure which follows the valve consists of the LEED gun and the lenses which focus the beam to the 0.5-mm aperture at the entrance of the LEED gun.

beam is injected into the deflector as a low divergence beam, appearing to come from a virtual cathode 3 mm behind the actual emitting surface. The real image which serves as the object for the subsequent beam transport and focusing system is formed several centimeters from the exit plane of the deflector.

The electron optical calculations in the cathode region were done by solving Laplace's equation numerically on a fine mesh with a high degree of accuracy; rays were subsequently traced using electric fields calculated from the stored mesh potentials. First-order approximations were not used since the initially assumed beam divergence of $\pm 40°$ far exceeded the small-angle or paraxial approximation criterion. Where analytical and simplified methods could be applied to calculated beam transfer through the extraction region, excellent agreement was obtained. The beam envelope shown in Fig. 10 is for an emitting energy of 0.3 eV; the trajectory calculations, however, were done individually for each energy component.

In principle, the 90° spherical deflector can also be used to monochromatize the beam. This would require different injection optics, a lower pass energy, an aperture at the image point after the deflector exit plane, and a sacrifice of beam current. However, the energy distribution of the beam is already sufficiently narrow for present experiments.

3. *Transport and focusing system*

The 1000-eV electron transport energy in the region of the valve was chosen to minimize the angular divergence of the beam over the long distance through the valve, and minimize the effect of stray magnetic fields while providing the possibility of focusing the beam through small apertures should differential pumping be required. The overall view of the electron optics is shown in Fig. 11.

In one version of the design, the beam transport system in the postdeflector region consisted of two segments separated by a 1-mm diameter beam-defining aperture labeled on Fig. 11 as optional. The design aim was to accelerate the beam to 1000 eV and then focus it without losses through this aperture. We have used the apparatus in this mode but now operate in a second mode with the aperture removed. This relaxes the stringent beam focusing requirements; as can be seen from Fig. 11, in this version the beam is transported in the field-free space in the valve with a very small divergence angle without a sharply defined crossover at the former beam-defining aperture location. Beyond the point of this optional aperture, an assembly of three equal-diameter bipotential lenses was used to produce a beam focus at the entrance to the LEED gun.

The focusing lenses in the beam transport system are accelerating or decelerating equal-diameter bipotential lenses, where the cylinders in each lens are spaced one-tenth of the lens diameter from each other. The focusing properties of a general equal-diameter bipotential lens have been calculated[69] using highly precise numerical techniques for sufficiently many discrete voltage ratios from 1.1 to 10 000 for both accelerating and decelerating modes. These focusing properties are available for

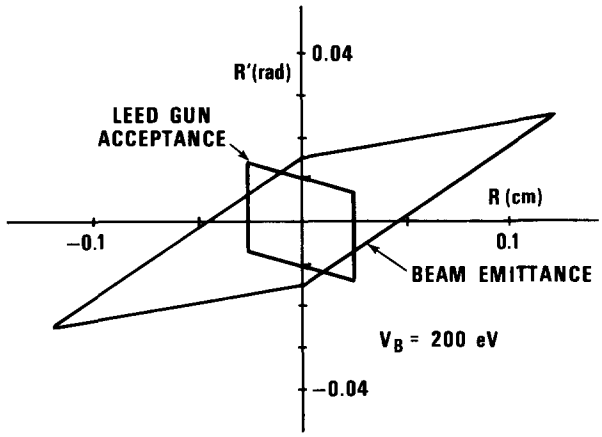

FIG. 12. The acceptance phase space area of the LEED gun is geometrically determined by the LEED gun apertures. The emittance phase space area of the beam shown for $V_B = 200$ eV increases at lower beam energies, since $\epsilon_{inv} = \sqrt{E}\,R'R$ = const, and below $V_B \sim 100$ eV completely overlaps the LEED gun acceptance area. The transmission decreases with decreasing energy because much less of the beam can be accepted by the LEED gun.

ray tracing as tabulated transfer matrix elements. They are stored in normalized units, permitting the use of any diameter lenses in any combination. With spline-fit interpolation between tabulated values, focusing properties can be calculated for any voltage ratio in the indicated range. First-order methods have been used to design and evaluate the beam transport and focusing system beyond the 90° deflector. We have taken care, however, to make certain that the maximum beam diameter in any given lens does not exceed 50% of the lens inner diameter. With this restriction aberrations are not significant in the present system.

4. The LEED system

Our LEED gun was modeled after the gun it replaced. The principal features are two apertures which define the beam followed by a deceleration of the beam to give a nominal 2:1 change in the electron energy. The 2:1 ratio is designed to minimize the size of the beam at the Faraday cup or LEED screen in the presence of space charge and may differ somewhat from 2:1 depending on the energy and current of the beam.

We chose to have a system where the potentials on all lens elements in the region from the cathode up to the LEED gun entrance could be kept constant relative to the cathode; that is, the electron kinetic energy at each point in this region is independent of the beam energy V_B at the target. For the purposes of this discussion, we include the last lens before the 0.5-mm aperture as part of the LEED gun. It is at this lens that the electron kinetic energy varies when the beam energy (cathode potential) is varied. As the electron energy at the target changes from 1 to 250 eV the electron energy at this lens changes from 2 to 500 eV.

The coupling between the region where the electron energy is independent of the beam energy at the target and the region of variable energy requires a fixed-focus, variable-energy optical system. We have used the so-called "neck-lens" principle for the last lens before the aperture in order to achieve the fixed-focus condition over a substantial range of higher energies. The "neck-lens" principle is based on the fact that for a range of voltage ratios in a bipotential lens, i.e., from 2 to 20, a specifically selected object-image relationship can be maintained,[69] although the magnification does vary somewhat.

The LEED gun acceptance was determined by the two 0.15-cm apertures, spaced 2.2 cm apart. The phase space determined by these two apertures was then projected to the LEED gun entrance, and after superimposing the restriction of the 0.5-mm aperture, we obtain a geometrically defined phase-space product of 0.26×10^{-3} cm-rad. The actual shape of this phase-space area is shown in Fig. 12. The quantity which determines to what extent we can expect to match the beam emittance to the gun acceptance is the above phase-space product multiplied by the square root of the beam kinetic energy at which the matching is to take place. At high energies where there is the possibility of transmitting more of the beam through the LEED gun, the fixed-focus requirement of the last lens before the 0.5-mm aperture is stricter than at low energy. At energies below $V_B \sim 100$ eV, the fixed-focus requirement is somewhat relaxed by the fact that the emittance of the incident beam exceeds the LEED gun acceptance.

In order to calculate the maximum possible transmitted current for ideal matching, we assume the current is distributed uniformly in the occupied phase space and fills the entire LEED gun acceptance area so that the transmitted current is proportional to the square of the ratio of the acceptance phase-space area to emittance phase-space area. If all of the beam was emitted with a 0.35 eV energy from an area 1 mm in diameter, giving an emittance invariant of 0.0192 cm-rad-$eV^{1/2}$, and if the beam energy at the target was 200 eV giving an equivalent LEED gun acceptance invariant of 0.00525 cm-rad-$eV^{1/2}$, the amount of beam that could be accepted by the LEED gun would be 7.4%. (Note that the matching energy for calculating the LEED gun acceptance is twice the beam energy at the target.) If the currents were emitted at 0.25, 0.15, or 0.05 eV energies, the same calculation would predict the amount accepted by the LEED gun optics to be 11.3%, 17.8%, and 37.4%, respectively. Due to the large emission angles at the photocathode, the emittance (and hence the beam transmission) calculated by exact ray tracing differs slightly from the emittance calculated from a straightforward application of the emittance invariant. It is clear, however, that the final achievable current is critically dependent on the initial emission energy. Given the assumed energy distribution of the photocathode, the maximum achievable current transmission through the LEED gun at a 200-eV beam energy is calculated to be 13%. In fact, the focusing cannot be done perfectly, and certainly not in such a manner as to focus the various current components individually. It should be clear that quantitative beam transport calculations and matching with experiment

can only be as good as the precise knowledge of the initial beam parameters and their distribution in current and energy.

5. Deflection plates

Because real electron optical systems are not perfectly aligned and stray magnetic fields may be present, deflection plates are included in the system. The transmission is very sensitive to misalignment of the beam. For example, at the 0.5-mm entrance aperture of the LEED gun, where beam emittance-gun acceptance matching has been calculated as shown in Fig. 12, the acceptable angular spread of the gun acceptance is ±10 mrad.

Each set of deflection plates is incorporated within an individual lens element and is biased positive or negative with respect to that element. A single set of four deflection plates is used to make angular corrections, while a dual set of four plates permits a transverse displacement of the beam as well as an angular correction.

C. Construction and operation

1. Mechanical

As discussed previously, and depicted in Fig. 11, the electron transport system is divided into two parts, the source and the LEED gun including the three lenses before it. The break between these two corresponds to the placement of the isolation valve shown in Fig. 1. Each set of optics finds its mounting reference on a vacuum flange of its respective chamber. The chambers are linked together by the isolation valve, and care must be taken to achieve proper translational and angular alignment of the two axes of the two electron optical systems.

Since electrons in the valve region must be surrounded by an equipotential surface at a potential of 1000 V with respect to the cathode, a movable electrode was incorporated in the design. It is moved by an electrically isolated rack and pinion and closes the gap between the last element on the top of Fig. 11 and the first element on the bottom. It is retracted into the source when the isolation valve is to be closed.

The electron optical elements consist of tube lenses, four sets of four deflection plates, and a 90° section of a spherical deflector. All of the electron optical elements are made of copper, except for the apertures which are made of molybdenum. Circular collars of machineable glass ceramic support, center, and space the cylindrical lens elements. All of the lens elements are designed to overlap adjoining elements so that there is no line-of-sight for the electron beam to see an insulating surface and be affected by charging. A single layer of magnetic shielding, fabricated out of "Mu-metal" 1 mm thick, is mounted external to the source vacuum chamber. It attenuates the earth's magnetic field to a level of less than approximately 30 mG. The electron optics beyond the valve is inside the surface analysis chamber which has internal magnetic shielding and a residual field of about 5 mG.

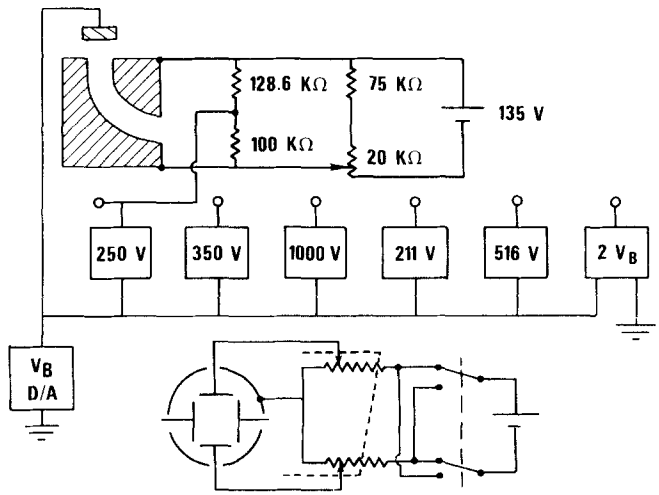

FIG. 13. A schematic of the potentials required. The beam energy relative to the target (at ground) is determined by the negative voltage applied to the GaAs photocathode by a computer controlled power supply (D/A). Individual power supplies referenced to the photocathode provide the voltages required by the lens elements. The voltage divider for the 90° spherical deflector is shown at the top of the figure, and a divider for a pair of deflection plates (shown schematically) is shown at the bottom of the figure.

2. Electrical

The potentials necessary to operate such an electron optical system are, in general, to be derived in one of two ways. Either a power supply is provided for each potential required, or a potential divider is constructed of resistive elements to provide all, or most, of the necessary potentials from a single voltage source. The former solution has the advantages of quick assembly time, low impedance outputs with the resultant freedom from some sources of interference, wider flexibility, and high speed programming of voltages. The latter has the advantages of smaller size, economy, and freedom from the cumulative effect of the noise levels of many power supplies. The typical system is usually a hybrid of the two, and such is the case for our instrument.

For our experiment, the target is at ground potential, so that the energy of the beam incident on the target is set by biasing the GaAs photocathode negatively by an equivalent amount. This is accomplished by a computer controlled digital-to-analog converter (D/A) as indicated in Fig. 13. The potentials of most of the lens elements are set by power supplies and are constant with respect to the cathode potential. The exception is a special voltage programmable supply[70] which maintains a potential equivalent to twice the beam energy at the next to the last gun element and provides the potential for the resistive divider which controls the last set of deflection plates.

The sphere potentials and the deflector plate potentials are derived from resistive dividers across the outputs of power supplies. These potentials are referenced to the potential of the surrounding lens element, or, in the case of the spheres, to the potential of the elements on either side. Thus, each of these power supplies could provide voltage to two, four, or eight elements, depending upon its use for the spheres, a set of deflectors, or a dual set

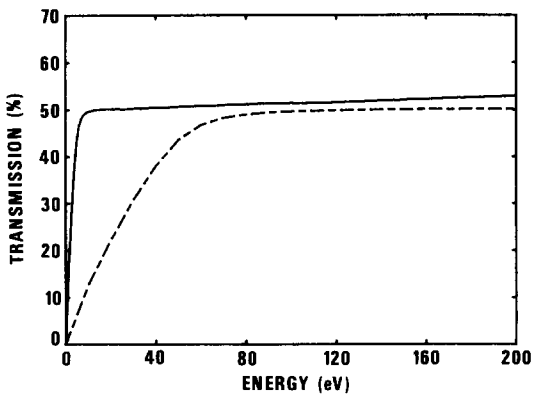

FIG. 14. The ratio of the total beam current passing through the 0.5-mm aperture to the total current leaving the photocathode is plotted as a function of electron beam energy. The low-energy part of the transmission given by the solid line is replotted as the dashed line. The horizontal energy scale for the dashed line runs from 0 to 20 eV.

of deflectors. An important caution here is that the use of a power supply (that is not highly isolated from ground), with neither output having a low impedance path to ground, can introduce a significant amount of noise at the power line frequency at the deflectors. This has been avoided here via the use of isolated power supplies. Other alternatives are battery power or filtering, which have the respective disadvantages of inconvenience and slow response time.

3. Tests of the electron optics

The objective of the electron optical design was to provide a high transmission while fulfilling the conditions necessary for the LEED experiments. It was also desirable that this transmission vary in a reasonably smooth manner as a function of beam energy. The solid line in Fig. 14 shows the transmission of the polarized electron source for electron beam energies between 0 and 200 eV as the beam energy is swept under the computer control. It represents the ratio of the total current passing through the 0.5-mm aperture to the total current measured leaving the photocathode. The dashed line shows the transmission with the beam energy on an expanded scale from 0 to 20 eV. Thus, the transmission through the 0.5-mm aperture is >50% above 10-eV beam energy. The electron beam is somewhat larger than the aperture, which makes the transmission less sensitive to small displacements of the beam. After the stringent requirements of the LEED gun are applied, overall transmissions of 1%, 5%, and 15% are measured for respective beam energies of 30, 100, and 200 eV, in reasonable agreement with our calculations.

The energy distribution of the electron beam was measured by using a small retarding field analyzer built into the LEED Faraday cup detector. The device has a stated[67] resolution ($\Delta E/E$) of less than 0.5%. By measuring the energy distribution of the incident beam at high incident energies where the observed full width at half-maximum is overwhelmingly due to the instrument resolution, we obtain experimentally 0.14% for the energy resolution of the energy analyzer. An energy distribution measurement taken at a lower incident energy, 50 eV, is shown in Fig. 15. Both the current variation with retarding field and its numerically obtained derivative are shown. The full width at half maximum of 0.15 eV is composed of a 0.07-eV contribution from the analyzer resolution and a 0.13-eV energy FWHM in the beam. These measurements were made with the GaAs cathode at −150 °C. A similar measurement at a cathode temperature of 26 °C gives a beam energy distribution width of 0.16 eV when the analyzer contribution is removed. Because of the sensitivity of this type of energy analyzer to angular dispersion within the incident beam, these measured values should be viewed as upper limits. The energy distribution shown is asymmetric with a tail to lower energies. This asymmetry results from electron–phonon scattering in the band-bending region as discussed in Sec. III.

V. PERFORMANCE

A. Summary of source parameters

The requirements of a polarized electron source were summarized in the Introduction. The parameters discussed were the polarization, the intensity, the reversibility of the polarization and the time structure of the reversibility, the polarization direction, the electron optical properties, and the stability. In this section, we review the parameters of our source and gather them together in Table I.

As pointed out in Sec. IIID the figure of merit, P^2I, often quoted for polarized electron sources depends on the light intensity in the case of a photoemissive cathode. In order to compare with other types of sources we can take a typical light intensity. For example, an intensity

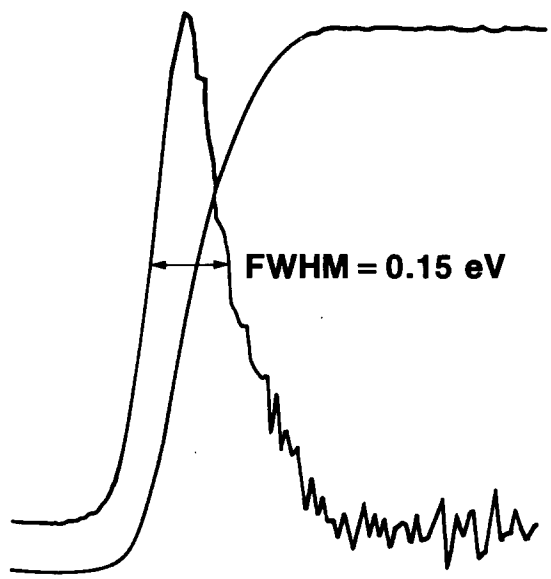

FIG. 15. The beam current collected by the Faraday cup is plotted as a function of retarding voltage on its retarding electrode. The derivative gives the energy distribution of the electrons. The low-energy tail on the right of the distribution is due to electron scattering with phonons in the band-bending region of the GaAs. During this measurement the GaAs was at a temperature of 110 K. When the contribution of the analyzer to the broadening is accounted for, the energy spread of the electron beam is 0.13 eV FWHM.

of 1 mW and the yield of 3% as in Fig. 8 gives a photocurrent of 20 μA. The polarization is typically 43 ± 2% for a NEA (100) GaAs photocathode at a temperature near 110 K and 36 ± 2% at room temperature. We do not have experience with higher light intensity; we would expect that much higher currents are attainable but that the source would have to be engineered to achieve an acceptable stability as described below.

In our source design, the initial longitudinal polarization of the beam is transformed to transverse polarization by a 90° electrostatic deflection. The polarization modulation can have arbitrary time structure; our rotating quarter wave plate produces a sinusoidal variation of the electron beam polarization at 30 Hz. The electron beam intensity remains constant while the polarization is modulated.

The electron beam starts at low energy of ~0.25 eV from a small area of ~0.5-mm diameter on the cathode surface and is emitted into an estimated cone half-angle of 30°. The source is electron optically bright as seen from an estimate of the phase space product $EA\Omega = 0.043\ \text{eV}\cdot\text{mm}^2\cdot\text{sr}$. A brighter source can be obtained with a smaller light spot. The energy spread of the beam was found to be 130 meV FWHM at 120 K.

The stability of the electron beam intensity and polarization are important considerations, especially when considering scaling the source to high intensities. The short-term intensity stability is excellent provided the light spot does not move on the photocathode surface (Sec. IC), the electron beam is well focused, and lens and deflection plate voltages have minimum ripple. Without extraordinary precautions we can measure spin dependent scattering intensities at a noise level of less than 5×10^{-4} of the spin-independent intensity. This represents an upper limit on spurious fluctuations in the beam intensity at the signal frequency.

In the long term, we find that the intensity decays to $1/e$ of its value in 4–12 h. The polarization, on the other hand, remains constant; cathode stability as used here refers to the stability of the electron beam intensity. The intensity can be brought back to its original value by warming the photocathode to room temperature or warming to room temperature and adding Cs. The fact that warming to room temperature can rejuvenate the cathode suggests that the low-temperature adsorption of impurities on the cathode may be a cause of the reduced intensity. The SLAC group[13] found that their source intensity half-life could be increased to 24 h if the apparatus in line of sight of the cathode was cooled to liquid nitrogen temperature. We have provided for cooling of the aperture and outer spherical deflector which are the main parts seen by our cathode. The few lifetime tests we made with such cooling were inconclusive, however, apparently due to the larger effect of electron stimulated desorption (ESD) of ions and neutrals from electrodes in the electron beam path. These can readsorb on the emitting surface or, in the case of ions, actually sputter the emitting surface. Such effects have been observed in the operation of GaAs cold cathodes.[71]

TABLE I. Summary of source parameters.

Polarization	photocathode temperature	110 K	43 ± 2%
		300 K	36 ± 2%
	transverse easily reversible		
	modulation frequency		30 Hz
Intensity	1 mW incident radiation		20 μA
Stability	I	half-life: 4–12 h	
	P	constant	
Electron optical	E_0		0.25 eV
	ΔE		0.13 eV FWHM
	$EA\Omega$		0.043 eV·mm²·sr

We found that, by lowering the accelerating voltage to the first aperture, below the 17.6 eV threshold for ESD of O^+ from polycrystalline molybdenum,[72] the cathode lifetime was increased even though approximately 25% of the beam hit the first aperture under these conditions. However, for best beam behavior we operate at the design voltage of 250 V on the first aperture. If more beam current is required when the cathode has decayed after a period of measurement, we remove neutral density filters from the incident light beam. We generally find a correlation between the cathode lifetime and beam current; that is, the lifetime is shorter for higher currents presumably due to correspondingly larger ESD. A more sophisticated extraction electrode structure in front of the photocathode would reduce the ESD and improve stability. We have not pursued this because the source already operates very satisfactorily for our polarized low-energy electron scattering measurements.

B. Application of the source

We have used our polarized electron source for polarized low-energy electron diffraction (PLEED) measurements of surfaces, which we illustrate briefly here. The source described in this paper has an extremely wide range of applications with some adaptation of the light and electron optics to special circumstances. For example, a 20-GeV polarized electron beam was obtained using such a source at SLAC.[13,16]

For low-energy electron scattering from surfaces, the important terms in the interaction Hamiltonian are

$$H_{\text{int}} = \sum_i V(\mathbf{r} - \mathbf{r}_i) + (1/2m^2c^2) \sum_i (\mathbf{r} - \mathbf{r}_i)^{-1} \times (dV(\mathbf{r} - \mathbf{r}_i)/dr)\mathbf{s}\cdot\mathbf{L} + \sum_i J(\mathbf{r} - \mathbf{r}_i)\mathbf{s}\cdot\mathbf{S}_i \quad (12)$$

where $V(\mathbf{r} - \mathbf{r}_i)$ and $J(\mathbf{r} - \mathbf{r}_i)$ are, respectively, the Coulomb and exchange potentials between an incident electron of spin $\mathbf{s}$ at $\mathbf{r}$ and an atom at $\mathbf{r}_i$. $\mathbf{S}_i$ is the spin of the atom and $\mathbf{L}$ is the orbital angular momentum of the scattered electron. The first term gives rise to spin-independent scattering. The second term, the spin–orbit interaction, is proportional to the gradient of the Coulomb potential and depends on the relative orientation of the incident spin polarization and $\mathbf{L}$. The third term is the exchange interaction which only gives a spin-dependent scattering for the case of a magnetic material.

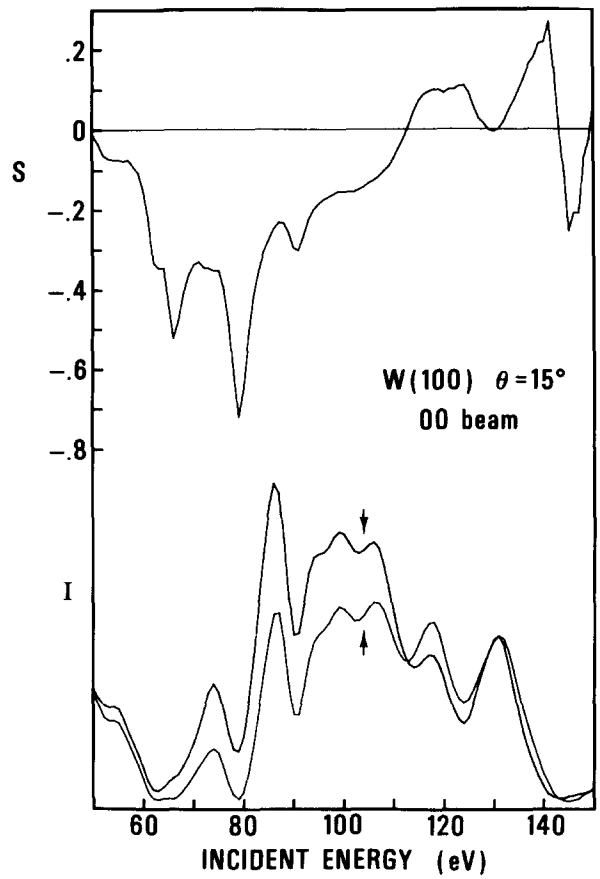

FIG. 16. Scattering from a W(100) surface shows a strong spin dependence in the scattering due to the interaction of the electron spin with its orbital angular momentum as it scatters from an atom in the surface. Specular scattering at an angle of incidence of 15° is shown as an example. The cross sections for scattering spin-up electrons $I\uparrow$ and spin down electrons $I\downarrow$ are shown at the bottom of the figure. These differ by a factor of 6 at 79 eV and by almost a factor of 2 near the 80-eV maximum. At the top of the figure we plot $S = (I\uparrow - I\downarrow)/(I\uparrow + I\downarrow)$.

We have measured spin dependent scattering from the (100) face of W.[14] The measured quantity S is the intensity for s parallel to L minus the intensity for s antiparallel to L, normalized to the sum of the two intensities. (For the purpose of this discussion we assume single scattering and L determines the normal to the scattering plane.) The ac component of the scattered current synchronous with the spin modulation of the incident beam is measured with a lock-in amplifier and is the spin-dependent signal. The dc component of the scattered intensity is the spin-independent signal. S is just the ratio of the ac to dc signal, corrected for the fact that the incident polarization is less than 100%. An example of such a measurement is shown in Fig. 16; S is measured for specular diffraction from W(100) at an angle of incidence of 15° in the (010) azimuth. Below S we have plotted what the scattered intensity would be if the incident polarization were entirely spin up ↑ or spin down ↓. Spin dependent effects can be very large; at the 79 eV minimum $I_\downarrow$ is over 6 times $I_\uparrow$ and even at the 86 eV maximum $I_\downarrow$ is approximately twice $I_\uparrow$. A 100-eV scan with data accumulated at 1-eV intervals as in Fig. 16, takes 3 min. Currents at the W crystal of the order 10^{-7} A are adequate for such measurements. We are currently determining the usefulness of data of this type in a surface structure determination.

In the case of scattering from a ferromagnetic Ni surface, we choose the incident spin polarization direction so that s is perpendicular to L in order to observe the spin dependence due to the third term in Eq. (12). Then S is the normalized intensity difference for incident P parallel and antiparallel to the spins S_i in the surface. It is possible to measure the temperature dependence of the surface magnetization and surface magnetization hysteresis curves.[15] For a surface magnetization hysteresis curve, instead of varying the incident beam energy as in Fig. 16, the energy E is fixed and S is measured as the magnetic field is varied. An example of $S(H)$ is shown in Fig. 17 for the specular beam at an intensity peak at $E = 125$ eV and at an angle of incidence of 12°. The precise measurement of such small polarizations illustrates the extraordinary advantages of this type of polarized electron source.

C. Comparison with other sources

There have been a number of papers in which comparisons of spin polarized electron sources have been made.[3,5,11,73–76] No attempt will be made here to give a detailed review, but rather to provide some perspective by gathering together parameters of some competitive sources in Table II. The sources can be categorized roughly into solid state sources and atomic sources. In the solid state category, there are sources utilizing photoemission from NEA and PEA GaAs, photoemission from ferromagnetic EuO,[6] and field emission from W tips coated with magnetized EuS.[5] In the atomic physics category, there are sources utilizing an optically pumped He discharge,[1] photoionization of Rb[2] and Cs[3] with circularly polarized light (Fano effect), and photoionization (with unpolarized light) of a polarized Li beam.[4] In Table II, we do not include the polarization of an elec-

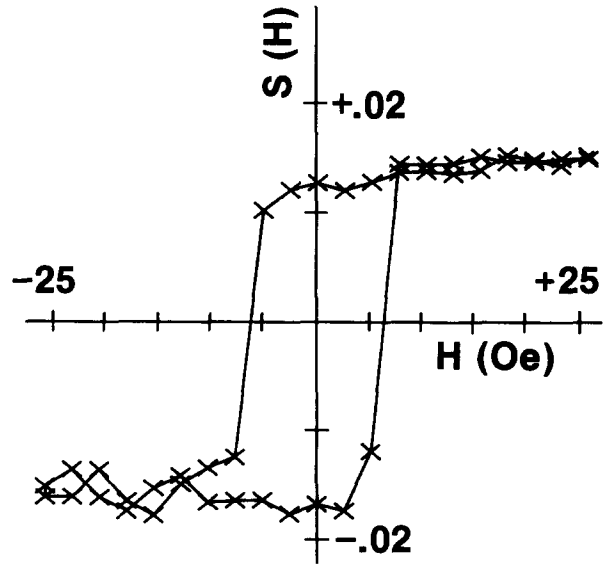

FIG. 17. The surface magnetization hysteresis curve $S(H)$ for Ni(110) is shown for specular scattering of a 125-eV beam at angle of incidence of 12°. At this energy, $S(H)$ is proportional to the magnetization of the outer two atomic layers.

TABLE II. Comparison of polarized electron sources.

Method	Group	Ref.	P	Polarization reversal	I_{dc} (μA)	I_{pulse} (el/pulse) (rep. rate)	ΔE (eV)	$EA\Omega$ (eV·mm²·sr)
Photoemission from NEA GaAs (100)	NBS	this work	0.43	optical	20[a]		0.13	4.3×10^{-2}
	SLAC	13	0.43	optical		10^{11}/1.5 μs 120 Hz	0.13	
Photoemission from PEA GaAs (110)	ETH-Zurich	66	0.35	optical	4[a]		0.3	
Photoemission from EuO	ETH-Zurich	6	0.61	magnetic field	1	3×10^9/1.5 μs	2	1.8×10^5
Field emission from W-EuS	Bielefeld	5	0.85	magnetic field	0.01		0.1	1.9×10^{-9}
Optically pumped He discharge	Rice	1	0.40	optical	2		0.15	1.6
Fano effect, Rb	Bonn	2	0.65	optical		2.2×10^9/12 ns 50 Hz	<500	1.1×10^2
Fano effect, Cs	Yale	3	0.63	optical	0.01		3	3.9×10^2
Photoionization polarized Li	Yale	4	0.85	magnetic field		2×10^9/1.5 μs 180 Hz	1500	$<6.4 \times 10^3$

[a] for 1 mW incident light power.

tron beam on scattering due to the spin–orbit interaction such as in scattering from a Hg beam[77] or from a W surface.[14,63] As can be seen from Fig. 16, there are energies where high polarization can be achieved, but to reverse the polarization the beam energy or scattering angle must be varied, which is a disadvantage for most experiments. The intensity of a polarized scattered beam is decreased from the space charge limited current of the incident beam by the reflection coefficient of the crystal. Polarized electron sources based on scattering are inherently less intense than the GaAs source where the intensity of the polarized beam can reach its space charge limited value.

In assessing a source of polarized electrons, the particular application must be kept in mind. A very high current source with low brightness may look like a low current source to an experiment with an electron optical system that has a small acceptance. On the other hand, a very high brightness source may have no advantage for an experiment with an electron optical system that has a large acceptance. The ability to reverse the polarization of the electron beam without otherwise affecting the beam is a very useful feature for most experiments. Therefore, sources in which the electron polarization can be reversed by modulating the circular polarization of the incident photoexciting light have an important advantage. The NEA GaAs (100) polarized electron source offers many advantages and, for a wide range of applications, is superior to other currently available sources.

ACKNOWLEDGMENTS

We have had helpful discussions with many colleagues over the course of development of the GaAs source. Many workers in the area of GaAs technology provided information on cleaning and activating GaAs crystals; we would especially like to acknowledge helpful discussions with L. W. James and F. Carlson. We have enjoyed the on-going fruitful discussions about source development with C. K. Sinclair and E. L. Garwin of SLAC. This work was supported in part by the Office of Naval Research.

APPENDIX: CHEMICAL CLEANING PROCEDURE

1. Ultrasonically clean four beakers, teflon tweezers, and graduated cylinder in trichloro-ethylene, acetone, and methanol.
2. Mix 4 : 1 : 1 of concentrated H_2SO_4, 30% H_2O_2 and H_2O by volume. Carefully add the H_2SO_4 to the H_2O_2 and H_2O to avoid excessive heating.
3. Mix 1 : 1 NaOH (1-*M* solution: 4 g NaOH to 100 ml H_2O) and H_2O_2 (0.76-*M* solution: 1 ml 30% H_2O_2 to 11.5 ml H_2O).
4. Ultrasonically clean crystal at low power (to avoid breaking) in trichloro-ethylene for 3 min. Decant new trichloro-ethylene and repeat three times.
5. Decant methanol three times. Ultrasonically clean crystal in methanol for 3 min. Decant methanol and repeat three times.
6. Blow dry with filtered dry N_2.
7. Etch in 4 : 1 : 1 etch at 50 °C for 3 min, face up. Agitate to keep fresh etch at surface.
8. Rinse in 10 changes of deionized water and decant six times with methanol. Blow dry with filtered dry N_2.
9. Make visual inspection at this point. If surface is not clean and shiny, start over with a new crystal.

10. Etch in concentrated HF for 5 min at room temperature.

11. Rinse twice in deionized water.

12. Etch in 1 : 1 solution (from step 3) for 1 min at room temperature.

13. Rinse five times in deionized water. Decant five times with methanol. Blow dry with filtered dry N_2 and install in vacuum system immediately.

Notes: We use electronic grade solvents. The etches are freshly mixed each time, although we have successfully used components, such as the 1 *M* NaOH or 0.76 *M* H_2O_2, that were prepared well ahead. Deionized water with a resistivity > 15 MΩ-cm is used. Each etch, steps 7, 10, 12, is ended by flushing the deionized water without intermediate exposure to air. Immediate installation in the vacuum system usualy means in practice about ½ h until pumpdown.

[a] NRC-NBS Postdoctoral Fellow 1976–1977; Present Address: Physics Department, University of Maine, Orono, ME 04473.

[1] L. A. Hodge, F. B. Dunning, and G. K. Walters, Rev. Sci. Instrum. **50,** 1 (1979).
[2] W. von Drachenfels, U. T. Koch, Th. M. Müller, W. Paul, and H. R. Schaefer, Nucl. Instr. Methods **140,** 47 (1977).
[3] P. F. Wainwright, M. J. Alguard, G. Baum, and M. S. Lubell, Rev. Sci. Instrum. **49,** 571 (1978).
[4] M. J. Alguard, J. E. Clendenin, R. D. Ehrlich, V. W. Hughes, J. S. Ladish, M. S. Lubell, K. P. Schüler, G. Baum, W. Raith, R. H. Miller, and W. Lysenko, Nucl. Instr. Methods **163,** 29 (1979).
[5] E. Kisker, G. Baum, A. H. Mahan, W. Raith, and B. Reihl, Phys. Rev. B **18,** 2256 (1978).
[6] E. Garwin, F. Meier, D. T. Pierce, K. Sattler, and H. C. Siegmann, Nucl. Instr. Methods **120,** 483 (1974).
[7] G. Feinberg, Phys. Rev. D **12,** 3575 (1975).
[8] E. Garwin, D. T. Pierce, and H. C. Siegmann, Swiss Physical Society Meeting, 26 April 1974; Helv. Phys. Acta **47,** 393 (1974).
[9] D. T. Pierce, F. Meier, and P. Zürcher, Phys. Lett. A **51,** 465 (1975).
[10] D. T. Pierce, F. Meier, and P. Zürcher, Appl. Phys. Lett. **26,** 670 (1975).
[11] D. T. Pierce and F. Meier, Phys. Rev. B **13,** 5484 (1976).
[12] M. Campagna, D. T. Pierce, F. Meier, K. Sattler, and H. C. Siegmann, Adv. Electron. Electron Phys. **41,** 113 (1976).
[13] C. K. Sinclair, E. L. Garwin, R. H. Miller, and C. Y. Prescott, AIP Conf. Proc. **35,** 424 (1976); E. L. Garwin, R. H. Miller, C. Y. Prescott, C. K. Sinclair, and M. Borghini, to be published.
[14] G.-C. Wang, B. I. Dunlap, R. J. Celotta, and D. T. Pierce, Phys. Rev. Lett. **42,** 1349 (1979).
[15] R. J. Celotta, D. T. Pierce, G.-C. Wang, S. Bader, and G. Felcher, Phys. Rev. Lett. **43,** 728 (1979).
[16] C. Y. Prescott, W. B. Atwood, R. L. A. Cottrell, H. DeStaebler, E. L. Garwin, A. Gonidec, R. H. Miller, L. S. Rochester, T. Sato, D. J. Sherden, C. K. Sinclair, S. Stein, R. E. Taylor, J. E. Clendenin, V. W. Hughes, N. Sasao, K. P. Schuler, M. G. Borghini, K. Lübelsmeyer, and W. Jentschke, Phys. Lett. B **77,** 347 (1978).
[17] D. T. Pierce, C. E. Kuyatt, R. J. Celotta, Rev. Sci. Instrum. **50,** 1467 (1979).
[18] D. T. Pierce, G.-C. Wang, and R. J. Celotta, Appl. Phys. Lett. **18,** 220 (1979).
[19] Sylvania C100 P, the so-called "Western Union" lamp, 100 W. Certain commercial equipment, instruments, or materials are identified in this paper in order to more clearly describe our apparatus. In no case does such identification imply recommendation or endorsement by the National Bureau of Standards, nor does it imply that the material or equipment identified is necessarily the best available for the purpose.
[20] Schott RG 715.
[21] M. Born and E. Wolf, *Principles of Optics* (MacMillan, New York, 1964), 2nd ed., p. 524.
[22] D. Nyyssonen, private communication.
[23] Laser Diode Labs. LCW-10; RCA 30130.
[24] The assistance of A. W. Hartman is gratefully acknowledged.
[25] Polaroid type HN 7.
[26] J. C. Kemp, J. Opt. Soc. Am. **59,** 950 (1969).
[27] U. Heinzmann, J. Phys. E **10,** 1001 (1977).
[28] *RCA Electro-optics Handbook* (RCA, Commercial Engineering Harrison, N.J., 1968).
[29] We thank Fred Carlson, Night Vision Laboratory, Ft. Belvoir, VA, for his assistance.
[30] We thank B. J. Waclawski for designing and assembling this manipulator.
[31] W. Klein, Rev. Sci. Instrum. **42,** 1082 (1971).
[32] J. J. Scheer and J. van Laar, Solid State Commun. **3,** 189 (1965).
[33] R. L. Bell, *Negative Electron Affinity Devices* (Clarendon, Oxford, 1973).
[34] W. E. Spicer, Appl. Phys. **12,** 115 (1977).
[35] M. Erbudak and B. Reihl, Appl. Phys. Lett. **33,** 584 (1978).
[36] Laser Diode, Inc., sodium hypochlorite polish.
[37] L. W. James, G. A. Antypas, J. Edgecumbe, R. L. Moon, and R. L. Bell, Appl. Phys. **42,** 4976 (1971).
[38] A. U. MacRae, Surf. Sci. **4,** 267 (1966).
[39] J. R. Arthur, Surf. Sci. **43,** 449 (1974).
[40] J. E. Rowe, private communication.
[41] B. J. Stocker, Surf. Sci. **47,** 501 (1975).
[42] B. Goldstein, Surf. Sci. **47,** 143 (1975).
[43] We thank H. Schade for making a piece of this material available to us.
[44] J. J. Uebbing, J. Appl. Phys. **41,** 802 (1970).
[45] S. Iaida and K. Ito, J. Electrochem. Soc. **118,** 768 (1971).
[46] I. Shiota, K. Motoya, T. Ohmi, N. Miyamoto, and J. Nishizawa, J. Electrochem. Soc. **124,** 155 (1977).
[47] C. T. Foxon, J. A. Harvey, and B. A. Joyce, J. Phys. Chem. Solids **34,** 1693 (1973).
[48] B. Goldstein, D. J. Szostak, and V. S. Ban, Surf. Sci. **57,** 733 (1976).
[49] D. G. Fisher, IEEE Trans. Electron Devices **ED-21,** 541 (1974).
[50] C. Piaget, "Electronic Emission Properties of III–IV Semiconductors in a State of Negative Electron Affinity," Ph.D. Thesis, Université Paris, Sud, Centre d'Orsay, 1977.
[51] W. E. Spicer, Phys. Rev. **112,** 114 (1958).
[52] L. W. James and J. L. Moll, Phys. Rev. **183,** 740 (1969).
[53] Presented in Ref. 33, Appendix C.
[54] D. J. Bradley, M. B. Allenson, and B. R. Holeman, J. Phys. D **10,** 111 (1977).
[55] For reviews see: B. P. Zakharchenya, *Proceedings of the Eleventh International Conference on the Physics of Semiconductors, Warsaw, 1972*, edited by M. Miasek (PWN-Polish Scientific, Warsaw, 1972), p. 1315; and G. Lampel, *Proceedings of the Twelfth International Conference on the Physics of Semiconductors, Stuttgart, 1974*, edited by M. H. Pilkuhn (Teubner, Stuttgart, 1974), p. 743.
[56] G. Fishman and G. Lampel, Phys. Rev. B **16,** 820 (1977).
[57] G. L. Bir, A. G. Aronov, and G. E. Pikus, Zh. Eksp. Teor. Fiz. Sov. Phys. JETP **42,** 705 (1976).
[58] A. H. Clark, R. D. Burnham, D. J. Chadi, and R. M. White, Sol. State Commun. **20,** 385 (1976).
[59] M. I. D'yakonov and V. I. Perel', Zh. Eksp. Teor. Fiz. Sov. Phys. JETP **38,** 177 (1974).
[60] John Malamas, private communication. We thank Dr. Malamas for providing his measurements of α at doping levels 4.4×10^{18} and 9.3×10^{18} cm^{-3} prior to publication.
[61] D. Z. Garbuzov, R. I. Dzhioev, L. M. Kanskaya, and V. G. Fleisher, Sov. Phys. Sol. State **14,** 1481 (1972).
[62] D. M. Campbell, H. M. Brash, and P. S. Farago, Phys. Lett. **31,** 499 (1971).
[63] M. Kalisvaart, M. R. O'Neill, T. W. Riddle, F. B. Dunning, and G. K. Walters, Phys. Rev. B **17,** 1570 (1978).
[64] M. G. Burt and J. C. Inkson, J. Phys. D: Appl. Phys. **10,** 721 (1977).
[65] I. Kudman and T. Seidel, J. Appl. Phys. **33,** 771 (1962).
[66] B. Reihl, M. Erbudak, and D. M. Campbell, Phys. Rev. B **19,** 6358 (1979).
[67] Varian, model 981-2125 gun in model 981-0137 LEED apparatus.
[68] E. M. Purcell, Phys. Rev. B **54,** 818 (1938).
[69] D. DiChio, S. V. Natali, and C. E. Kuyatt, Rev. Sci. Instrum. **45,** 559 (1974).
[70] Kepco, model NTC2000.
[71] H. Schade, H. Nelson, and H. Kressel, Appl. Phys. Lett. **20,** 385 (1972).
[72] P. A. Redhead, Can. J. Phys. **42,** 886 (1964).
[73] J. Kessler, *Atomic Physics 3*, edited by S. J. Smith and G. K. Walters (Plenum, New York, 1973), p. 523.
[74] V. W. Hughes, R. L. Long, Jr., M. S. Lubell, M. Posner, and W. Raith, Phys. Rev. **5,** 195 (1972).
[75] M. S. Lubell, *Atomic Physics 5*, edited by R. Marrus, M. Prior, and H. Shugart (Plenum, New York, 1977).
[76] R. J. Celotta and D. T. Pierce, "Sources of Spin Spolarized Electrons" in *Advances in Atomic and Molecular Physics*, edited by D. R. Bates and B. Bederson, (in press).
[77] K. Jost and J. Kessler, Z. Phys. **195,** 1 (1966).